Volume 1 | Number 1 | Jan 2013 | Pages 1–100

Soft Matter

www.rsc.org/softmatter

ROYAL SOCIETY OF CHEMISTRY

ROYAL SOCIETY OF CHEMISTRY

www.rsc.org/softmatter

Soft Matter   FULL PAPER SUBMISSION

Where physics meets chemistry meets biology for fundamental soft matter research

Soft Matter has a global circulation and interdisciplinary audience with a particular focus on the interface between physics, biology, chemical engineering, materials science and chemistry.

The following paper has been submitted to *Soft Matter* for consideration as a **full paper**.

Soft Matter aims to publish **high quality** papers reporting on the generic science underpinning the properties, applications, and phenomena of soft matter. The primary criterion for acceptance of a contribution for publication is that it must report high-quality new science and make a significant contribution to its field. *Soft Matter* is an **interdisciplinary** journal and suitable papers should cross disciplines or be highly significant within the field from which they originate.

Routine or incremental work, however competently researched and reported, should not be recommended for publication if it does not meet our expectations with regard to novelty and impact.

Thank you for your effort in reviewing this submission. It is only through the continued service of referees that we can maintain both the high quality of the publication and the rapid response times to authors.

We would greatly appreciate if you could review this paper in **two weeks**. Please let us know if that will not be possible. Please support all comments with scientific justifications or we may be unable to use your report/ask for extra feedback.

Once again, we appreciate your time in serving as a reviewer. To acknowledge this, the RSC offers a **25% discount** on its books: http://www.rsc.org/Shop/books/discounts.asp. Please also consider submitting your next manuscript to *Soft Matter*.

Best wishes,

Liz Dunn, Editor, *Soft Matter*

Dear Dr. Fisher,

Thank you very much for your kind note. We appreciate your efforts in handling this manuscript very much.

We would like to thank the Reviewers for their careful reading of the manuscript and their thoughtful comments. We have revised the manuscript according to the comments from the reviewer. Details of the revisions and our responses to the reviewer's comments are given below. For clarity, each comment of the Reviewers is repeated below, followed immediately by our response.

We hope that the revision and responses are satisfactory and our paper can be accepted in its current form.

Baohui Li
BinYu

Reviewer: 1

(1) In my opinion,

In this manuscript, the authors investigated the self-assembly of linear triblock copolymers confined in spherical nanopores using a simulated annealing method. They systemically studied the effects of pore diameter, pore-wall selectively, and copolymer composition on the formed patchy structures. While their work is interesting and solid, the following issues should be addressed before publication.

1. In the model section, the authors may want to include a brief description on the simulated annealing method. How does it work in principle? What software/package was used for computation and visualization?

Following this comment, we have added a brief description of the simulated annealing method in Pages 5 and 6 of the revised the manuscript. The simulations were carried out using Fortran 90 codes developed in house. The same codes have been used extensively in previous studies. We use the Mayavi software, which is in public domain, for the visualization.

2. On Page 8, please define the parameter x.

The parameter χ is defined in Page 7 of the revised the manuscript.

3. In the bulk morphology study, the authors used $\varepsilon AB = \varepsilon AC = \varepsilon BC$ and they found that their results were consistent with the type II frustration system, in which $\chi AC << \chi AB = \chi BC$. How does the relation $\varepsilon AB = \varepsilon AC$ lead to $\chi AC << \chi AB$?

The relation $\varepsilon_{AB} = \varepsilon_{AC} = \varepsilon_{BC}$ cannot lead to $\chi_{AC} << \chi_{AB}$. The interactions in our system are different from that in F^0, F^1 and F^2 systems. However, for the special case with $f_A = f_B = f_C$, lamellar phase is formed in all F^0, F^1 and F^2 systems, as well as our system, indicating that it is insensitive to the types of frustration.

4. On page 9, what would happen if the ratio D/Lo goes below 0.7?

When $D/L_0 < 0.7$, Janus nanoparticles, similar to that obtained at $D/L_0 = 0.7$, are obtained in our simulations. We have changed $D/L_0 = 0.7$ to $D/L_0 \leq 0.7$ in the revised the manuscript.

5. In Table 1, the authors presented the occurring probabilities of different patchy structures at D/Lo =1.4. It could be interesting to calculate the occurring probabilities of a specific patchy structure at various ratios of D/Lo to examine how the occurring probability changes with the ratio of D/Lo.

We agree with the Reviewer that calculating the occurring probabilities of specific patchy structures at various ratios of D/L_0 is a good idea. However, carrying out such calculations for every case demands a very long computing time. As mentioned in our manuscript, several different random number generator seeds (usually <10) have been performed to test the robustness of the observed self-assembled morphologies for all the simulations. For the calculation of the occurring probability of a specific patchy structure at $D/L_0 = 1.4$, we carried out more than one hundred simulations starting from different initial configurations to obtain a probability distribution. Such simulations are time-consuming. On the other hand, degenerated patchy structures seldom occur at other pore diameters, so we believe it is not necessary to calculate the occurring probabilities at various ratios of D/L_0.

6. In Figure 3, why is the surface-covered percentage different for A and C although the interactions between the pore-wall and either of them are the same?

The difference of the surface-covered percentages between A and C is due to the asymmetry of their domain structures. The asymmetry of their domain structures comes from the pore-wall preferences to the terminal A and C blocks and the chain structure of the block copolymer. The topological constraint of the chain structure tends to result in a concentric arrangement of A-B-C domains. On the other hand, the pore-wall preferences to the terminal A and C blocks tend to result in non-concentric arrangement on particle surface. The competition between these two factors results in patchy particles. In a patchy particle, A-patches and C-matrix occur on the particle surface and partially concentric arrangement of A-B domains occurs in the core. For a patchy particle, the total surface area of patches can be much smaller than the area of the matrix. Therefore, the surface-covered percentages for A and C are different. It can be deduced that if the total surface area of patches is equal to the area of the matrix in a patchy particle, there will be more A- C contact in the surface layer than that in the case when the area of patches is much smaller than that of the matrix. So, patchy particles with equal areas of patches and matrix are energetically unfavorable.

7.   In Figure 5, why is the mean squared end-to-end distance for D/Lo > 1.8 larger than that for the bulk phase?

The structure of a patchy particle is quite different from the bulk lamellar phase due to the strong pore-wall preference to the terminal A and C blocks. In a patchy particle, the A-domain (patches) distributed from the center to the surface of the particle. Therefore, when $D/L_0 > 1.0$, the size of A-domain will be larger than that in the bulk phase, and A-blocks will be stretched than that in the bulk phase. Such an assumption has been demonstrated in Figure 9b of our manuscript, where the mean-square end-to-end distances for every blocks are plotted as a function of α_A for the case of $\alpha_A = \alpha_C$, and $D/L_0 = 1.3$. In this relatively smaller pore diameter ($D/L_0 = 1.3$) case, it is noticed that A-blocks are stretched than that in the bulk phase. When $D/L_0 > 1.8$, the size of the A-domain is much larger than that the bulk phase. Therefore, it is deduced

that A-blocks are highly stretched than that in the bulk phase, which results in that the mean squared end-to-end distance for $D/L_0 > 1.8$ is larger than that for the bulk phase.

Reviewer: 2

In their work, the authors studied the self-assembly of linear ABC triblock copolymers confined in spherical nanopores, focusing on the case where the pore walls were attractive to both terminal blocks, and observed the formation of patchy nanoparticles. The authors performed a thorough study to quantify the effect that the pore size, pore wall selectivity and block copolymer composition would play on the self-assembled structures.

They concluded that the nanoparticle's number of patches increased with increasing the pore diameter or the wall selectivity, whereas the patches's shape was affected by the block copolymers composition.

COMMENTS

1- Can the authors comment on how the shape of the confinement might affect the resulting patchy particles?

This is an interesting observation. Based on our previous study of diblock copolymers under different shaped boundary confinement (Soft Matter, 2011, 7, 10227), such as a spherical or an ellipsoid pore, we can conclude that the shape of the confinement may have large effect on the structure of the resulting patchy particles. Carrying out simulations on various shaped cavities is an interesting research problem, but this is beyond the scope of the current study.

2- Can the authors explain the reason why they never observed particles with three patches, as stated at page 8 in the main text?
("On the other hand, particles with three patches have never been observed").

We should clarify that particles with three patches (P3) have never been observed for systems (with a fixed surface preference) studied in Section B. We clarify this in the revised manuscript. Actually P3 particle occurs for systems (with changing the

strength of the surface preference) studied in Section C. Our results demonstrate that the number of patches in a particle depends both on the pore diameter and the strength of the surface preference. For systems studied in Section B, the fixed surface preference value cannot result in a P3 particle.

Even though the results are clearly presented, the manuscript would highly benefit from a spelling check. Therefore, I suggest the authors to fix the typos that can be found throughout the paper in order to improve its quality.

Having spell-checked the manuscript and given possible answer to my comments, I suggest the manuscript for publication in Soft Matter.

We have revised the typos and improved the writing of the manuscript.

Patchy nanoparticles self-assembled from linear triblock copolymers under spherical confinement: A simulated annealing study

Bin Yu*, *Jianhua Deng*

Department of Physics and Material Science, Tianjin Normal University, Tianjin, 300387, China

Baohui Li *

School of Physics and Key Laboratory of Functional Polymer Materials of Ministry of Education,

Nankai University, and Collaborative Innovation Center of Chemical Science and Engineering

(Tianjin), Tianjin, 300071, China

An-Chang Shi

Department of Physics and Astronomy, McMaster University, Hamilton, Ontario L8S 4M1, Canada

---

* To whom correspondence should be addressed.

* E-mails: stevenyubin@163.com; (B.Y); baohui@nankai.edu.cn; (B.L.).

Abstract

The self-assembly of linear ABC triblock copolymers confined in spherical nanopores is studied using a simulated annealing technique. Morphological phase diagrams as functions of the pore diameter, the selectivity of the pore-wall to the terminal blocks, and the copolymer composition are constructed. A variety of patchy nanoparticles and multiple morphological transitions are identified. Janus nanoparticles, which can be regarded as particle with one patch, are observed inside small nanopores. With increasing the pore diameter, the number of patches on a nanoparticle surface increases from one to two, four, five, six, and seven. The size of each patch increases periodically. It is observed that the number of patches also increases with increasing the wall selectivity. The distribution of the patches on the surface of a given particle is highly symmetric. The interior structures of the patchy nanoparticles and the morphological transition are investigated by calculating the bridging fraction, the mean square end-to-end distance and the average contact number between different components. A series of entropy-driven morphological transitions is predicted. Furthermore, it is found the overall patchy morphology is largely controlled by the volume fraction of the middle B-block, while the internal structure is largely controlled by the volume fraction ratio of the two terminal blocks. Our study demonstrates that the size of nanopore, the pore-wall selectivity, and the copolymer composition could be utilized as effective means to tune the structure and properties of the anisotropic nanoparticles.

Introduction

The preparation of highly ordered and controllable nano-structures is a key target in modern material science and nanotechnology. In particular, fabrication of hierarchical structures from bottom-up self-assembling system to access versatile functional devices is a fundamental and promising topic in nanotechnology.[1-4] In recent years, anisotropic architectures such as patchy, multi-compartment and Janus particles have attracted tremendous attention due to their non-centrosymmetric features. Several review articles[5-10] have been published, focusing on the recent progresses in the preparation of those anisotropic particles and their applications. Janus particles, named after the two-faced Roman god, have a dipolar distribution of composition, functionality, chemistry, polarity, electrical and other properties. In contrast to Janus particles, patchy particles are characterized by multipolar surface patterns. Their highly anisotropic, directional interactions could drive the particles to form novel ordered structures.[11] One possible route to obtain patchy nanoparticles is to utilize multi-compartment micelles with hydrophilic shell and hydrophobic core, in which the core-components could phase-separate into individual sub-domains.[12] Due to the complex structures, anisotropic interactions and well-controlled patterns, those anisotropic nanoparticles have potential applications in switchable display device,[13] photonic crystal,[11] nano-containers as selective drug delivery,[14] and anisotropic building blocks for complex structures[3].

Due to their potential advanced applications, extensive theoretical and experimental studies of anisotropic patchy nanoparticles have been carried out. In a recent perspective article, Yoshida and Lahann described how "smart materials" could be used to facilitate complex functions.[15] They proposed that anisotropic nanoparticles with switchable-wall are promising candidates to access remarkable functions through hierarchical assembly. The progress made in recent synthesis and prognoses of anisotropic building blocks also has been discussed by Glotzer et al.[2, 3] Balazs and co-workers proposed a smart membrane material using amphiphilic Janus particles to open and close membrane pores.[16] Glotzer and co-workers showed that patchy particles with four patches located at the vertex of a tetrahedron can self-assemble into a diamond structure which could be used to fabricate three-dimensional photonic crystals.[17] Furthermore, in a Brownian dynamic study of hierarchical assembly of nanoparticles with variously distributed patches, Zhang *et al.* found that precise arrangement of patches combined with patch selectivity can be used to control the relative

position of particles and the overall assembled structures, demonstrating that multiple hierarchical structures including chains, sheets, tubes, and rings could be obtained.[11] Experimentally, anisotropic Janus particles have been successfully prepared and reported to self-assemble into spherical super-micelles[18, 19], order clusters[20, 21], flowerlike[22], tubular and sheetlike[23] superstructures. Despite these progresses, the fabrication of patchy particles with precise patterns remains a challenging task. In what follows we propose a route of fabricating patchy particles via confined self-assembly of block copolymers.

Block copolymers with their rich phase behavior have become a paradigm for the study of self-assembly.[24] In particular, micellar nanoparticles with multiple patches have also been prepared in experiments[25-30] and predicted in simulations in block copolymer solution systems.[31, 32] Srinivas and Pitera investigated a binary mixture of two different diblock copolymers in water using coarse-grained molecular simulations.[31] Their study showed that the shape, location, and the number and size of the patches can be controlled by changing the composition of hydrophilic versus hydrophobic, the interactions between blocks and solvent and the composition of copolymer mixture. In another study, Kong and co-workers simulated the self-assembly of amphiphilic ABC linear terpolymers in C-block selective solvent.[32] Various patchy micellar structures were observed which are controlled by the copolymer composition, copolymer concentration and incompatibility between the solvophobic blocks.

Besides the self-assembly of block copolymers in bulk, it has been shown that the combination of structural frustration, confinement-induced entropy loss and wall interactions in a spatially confined environment, provides opportunities to engineer novel structures which cannot access in the bulk.[33-45] Steward-Sloan and Thomas have reviewed the self-assembly of block copolymers under various types of confinement emphasizing experimental results and theoretical predictions.[46] Due to the richness of the confined self-assembly, it is expected that patchy nanoparticles can be obtained utilizing confined self-assembly of block copolymers. In general, for diblock copolymers confined in strongly preferential-wall environment, the surface of a self-assembled structure is covered by the wall-preferred monomers, thus forming core-shell type structures. Similarly, ABC triblock copolymers confined in nanopores with the wall preferring to the two terminal blocks would form core-shell type morphologies with the two terminal blocks in the shell. The microphase separation of the two terminal blocks in the shell could lead to the

formation of complex patchy structures, forming patchy nanoparticles.

Herein, we report a systematical study of the self-assembly of linear ABC triblock copolymers confined in spherical nanopores. We focus on the case that the pore-walls are attractive to both of the terminal blocks. Patchy nanoparticles spontaneously form due to the immiscible interactions between different blocks. The effects of the pore size, pore-wall selectivity and copolymer composition on the self-assembled structures are investigated. Phase diagrams as functions of various parameters are constructed. We find that properties of the self-assembled patchy nanoparticles such as the number, size, location, surface-covered percentage and the geometry of patches could be controlled precisely. Our study provides an effective route to engineer patchy nanoparticles with controllable properties. These patchy nanoparticles can serve as building blocks to fabricate functionally hierarchical structures.

Model and Method

In the current study, the self-assembly of linear ABC triblock copolymers confined in spherical nanopores is investigated using the simulated annealing method applied to the "single-site bond fluctuation" model of polymers.[47-49] The simulated annealing method is a well-known procedure for obtaining the lowest energy "ground states" of disordered systems.[50-53] Starting from an initial configuration, the ground state of the system is obtained by executing a set of Monte Carlo simulations at decreasing temperatures. Simulations at a given temperature correspond to a step. The temperature in the initial step is high enough to allow most of the trial moves to be accepted, and it is decreasing with a specified schedule in the following steps. The final configuration for a given step is subsequently taken as the starting point for the next step at a slightly lower temperature. At each step, enough trial moves are performed to allow the system to reach equilibrium at the corresponding temperature. This method provides a mechanism of escaping from local minima; hence the ground state of the system can be obtained at a low temperature. Our extensive previous studies have established that the simulated annealing method and the lattice model are appropriate for studying the self-assembly of block copolymers in confinement.[54-56] For completeness, the model and algorithm are reviewed briefly below.

The simulations are performed on a model system that is embedded in a simple cubic lattice of volume $V = L_X \times L_Y \times L_Z$. The model triblock copolymers used in the simulations are of the type

$A_{n1}B_{n2}C_{N-n1-n2}$, where $n1$, $n2$ and N are the number of the A, B and all monomers, respectively. The total monomer number in a chain is fixed at $N=24$ and the total monomer concentration in a model system is kept at a constant of $\rho=90\%$. Each monomer occupies one lattice site and the polymers are self- and mutual-avoiding. The bond length is set to be 1 and $\sqrt{2}$ lattice spacing, so that each site has 18 nearest-neighbor sites. For simulations of bulk systems, periodic boundary conditions are applied in all three directions, and we use boxes with $L_X \neq L_Y \neq L_Z$ to obtain the period of a bulk phase. For simulations of the confined systems, a spherical nanopore with diameter D is constructed from a box with $L_X = L_Y = L_Z = D+3$. The pore includes those lattice sites whose distance to the pore center is less than $D/2$, and these sites can be occupied by copolymers and vacancies. The lattice sites outside the pore constitute the pore-wall which cannot be occupied by the polymers.

In all cases, only nearest-neighbors interactions are considered. The repulsive interaction between any twokinds of speies is modeled by parameters $\varepsilon_{ij} = 1.0 k_B T_{ref}$, where $i, j =$ A, B , C, V (vacancy) or W (pore-wall), k_B is the Boltzmann constant and T_{ref} is a reference temperature. The A-A, B-B and C-C interactions are set to be zero, and interaction between a monomer and a vacancy is also set to be zero. The confining walls are chosen as neutral or preferential to the terminal A and C blocks with $\varepsilon_{AW} \leq 0$, $\varepsilon_{CW} \leq 0$, and they are always neutral to the middle B block with $\varepsilon_{BW} = 0$.

The start configuration is generated by putting an array of polymer chains onto the lattice. The polymer chains are parallel to one of the lattice axis. These chains are either in an extended or in one-fold conformation. Two types of trial moves, chain reversal and exchange moves, are used in the simulations, which are the same as those used in our previous studies. [54-56] Starting from the initial configuration at T = $30 T_{ref}$, the ground state of the system is obtained by a simulated annealing protocol with decreasing T by a factor of 0.95 at each step until 70 annealing steps are reached. At each annealing step, 25000 Monte Carlo (MC) steps are performed. One MC step is defined as the number of moves required, on average, for all the chains to be reversed and all the lattice sites to be visited once. Simulations with several different random number generator seeds have been performed to test the robustness of the observed self-assembled morphologies. Good reproducibility of the morphologies has been obtained.

Results and discussion

A. *Bulk morphology*

In our simulations, we focus on systems of linear triblock copolymers with equal block interactions, i.e., $\varepsilon_{AB} = \varepsilon_{AC} = \varepsilon_{BC} = 1.0 k_B T_{ref}$. The bulk morphology of the triblock copolymers is obtained in a rectangular box with volume $V = L_X \times L_Y \times L_Z$. The lengths of the box are varied so that the simulation box is commensurate to the period of the ordered structures. In all the cases, lamellar structures are obtained for triblock copolymers $A_8B_8C_8$. As shown in Fig.1, a lamellar structure with lamellae parallel to the x-y plane is obtained in a box with $V = 38 \times 40 \times 42$, in which the A-blocks are shown in red, the B-blocks in green and the C-blocks in blue. As can be seen from Fig.1, the triblock copolymers $A_8B_8C_8$ form a lamellar structure with the sequence of -AA-B-CC-B- which defines as one bulk period, L_0. Lamellae showing two periods are obtained in the z-direction. From these bulks simulations, the period of the lamellae is estimated to be $L_0 \approx 21$ lattice spacing.

The phase behavior of ABC triblock copolymers is complex due to the large number of governing parameters. Baily[57] suggested that triblock copolymer melts could be classified into three categories according to the relative strength of χ_{AC} compared to that of χ_{AB} and χ_{BC}, where χ is the Flory-Huggins interaction parameter. The three kinds of systems correspond to $\chi_{AC} >> \chi_{AB} \approx \chi_{BC}$, $\chi_{AB} < \chi_{AC} < \chi_{BC}$ or $\chi_{AB} > \chi_{AC} > \chi_{BC}$, and $\chi_{AC} << \chi_{AB} \approx \chi_{BC}$, and they are termed as non-frustration (F^0), type I frustration (F^1) and type II frustration (F^2) systems, respectively. The phase behavior of F^0 system has been investigated by Tyler *et al.* using self-consistent field theory (SCFT).[58] The phase behavior of the F^2 system has been examined by Guo *et al.* using SCFT with a generic Flourier-space approach.[59] F^1 systems have been studied experimentally by several research group.[57, 60-62], and theoretically by Sun *et al.*[63] For the special case with $f_A = f_B = f_C = 1/3$, lamellar phase is formed in all the F^0, F^1 and F^2 systems [58,59,63] Our observation that triblock copolymers $A_8B_8C_8$ form lamellar phase is consistent with all these studies, despite of the differences in χ values between theirs and ours. We have not carried out extensive simulations of bulk phases of the asymmetric copolymers. Their corresponding bulk phases can be roughly deduced from the phase diagram obtained in the reference 63, where for systems with $\chi_{AC} = \chi_{AB} = \chi_{BC}$ are studied.

B. *Confined morphologies of $A_8B_8C_8$ triblock copolymers*

In this section, we present the self-assembled morphologies of linear triblock copolymers

$A_8B_8C_8$ confined in spherical pores of different sizes when the pore-wall strongly prefers to the terminal A and C blocks ($\varepsilon_{AW}=\varepsilon_{CW}=-1.0k_BT_{ref}$). Confined morphologies as a function of the ratio of the pore diameter (*D*) to the bulk period, D/L_0 are given in Fig. 2, where snapshots of the overall view and the individual (A, B and C) domain structures are shown. An examination of the overall structures reveals that patchy particles always form when $D/L_0 \leq 1.8$ and the number of patches on a particle surface increases with the increase of the pore diameter. Due to the identical preference of the pore-wall to the two terminal blocks, both A and C domains are on the surface of the particles. It should be pointed out that the patches on the surface could be formed by either A or C blocks distributed in the C- or A-matrix, due to the fact that the pore-wall has the same preference to the terminal A and C blocks and A and C blocks have the same lengths. For simplicity, we refer the patch-forming block as the A-block in this case and in all of the following cases where the patches on the surface could be formed by either the A or the C blocks. As shown in Fig 2, when the pore is quite small at $D/L_0 \leq 0.7$, an interesting Janus nanoparticle is obtained. The particle can be regarded as a patchy structure with only one patch occupying half of the surface. In this structure, the middle B-blocks form an ellipsoid imbedded in the center of the particle. When D/L_0 is close to 1 ($D/L_0=0.8\sim1$), the A-blocks form a patchy structure with two circular patches distributed at the two poles of the particle surface, while the C domain evolves into a toroidal structure located at the equator of the particle surface, and the B domain evolves into a flat disk located at the center of the particle. For larger pores with diameters in the range of $D/L_0=1.1\sim1.8$, patchy structures with multiple patches spontaneously form. It is interesting to notice that particles with two (P2), four (P4), five (P5), six (P6) and seven (P7) patches occur at $D/L_0=1.1\sim1.4$, $1.4\sim1.6$, 1.7 and 1.8, respectively. On the other hand, particles with three patches have never been observed in the case considered in this section. The distribution of the patches at the particle surface is highly symmetric. We could construct a series of bipyramid by connecting the centers of the patches. For a structure with four and six patches, the centers of the patches locate on the vertexes of a regular tetrahedron and a regular octahedron, respectively. For a structure with five and seven patches, the centers of the patches locate on the vertexes of a triangular and a pentagonal bipyramid, respectively. As shown in Fig. 2, the C-blocks always form a layer of spherically perforated lamella located on the surface of the particle, while the middle B blocks form a cage-like structure with outward-warped caves imbedded inside the C-domain, thus separating the A and C domains. On the other hand, the

A-blocks form an interesting structure composed of a spherical-like core at the center of the particle, and several mushroom-like spikes. The top surface of each mushroom forms a patch on the surface of the particle and the root of a mushroom is a cylindrical channel connecting the surface patch and the centric core. When D/L_0 is close to 2 (D/L_0=1.9~2), it is found that patchy structures are replaced by structures with a hybrid of radiant cylinders and vaulted stripes on the surface. Furthermore, when D/L_0 is close to 2.5, structures with partially stacked disks are formed. These structures obtained at relatively larger pores are more close to the bulk lamellar phase than the patchy structures. Therefore, the patchy structures obtained at $D/L_0 \leq 1.8$ in our study can be regarded as highly frustrated structures which are very different from their bulk phase. It is interesting to notice that at a given pore size, we sometimes observe patchy structures with different number of patches or degenerated patchy structures, such as at D/L_0=1.4. Table I shows the probability of observing a particular structure among the degenerated structures at D/L_0=1.4, calculated based on more than one hundred simulations starting from different initial configurations. As shown in Table 1 and Fig. 2, we observed two stable structures, termed P4 and P5, at D/L_0=1.4, and two meta-stable structures, H1 and H2. H1 can be regarded as an intermediate transition structure from P4 to P5. H2 is a branching striped structure that seems like a claw. Both of the meta-stable structures, H1 and H2, relax to the stable P4 or P5 structure when we increase the MC steps. It is noticed that the preference of the P4 structure is slightly larger than that of the P5 structure at D/L_0=1.4. However, the P5 structure becomes the dominant morphology at D/L_0=1.5. This observation indicates that the number of patches on a particle surface increases with the increase of the pore size.

In order to gain some quantitative information about the patchy structures, the surface-covered percentages of A (SCP_A) and C (SCP_C) monomers, and the average surface-area occupied by A-monomers in one patch are calculated as a function of D/L_0. As shown in Fig. 3, although the interactions between the pore-wall and the two terminal blocks are the same, the resulting SCP_A and SCP_C are quite different. For a pore with D/L_0=0.7, both A and C monomers occupy 50% of the surface, corresponding to the Janus structures. However, for a larger pore, the SCP_A is always much smaller than SCP_C. The SCP_A value decreases from 50% to 45% in the range of D/L_0=0.7~1.0 corresponding to the morphological transition from the Janus nanoparticle to a nanoparticle with two patches. At D/L_0=1.0~1.8, the number of the patches increases from two to seven, while the

SCP_A decreases rapidly from 45% to 25%. It is interesting to notice that there is very small difference in the surface-covered percentages between the degenerate structures with four and five patches at D/L_0=1.4. This observation implies that the surface-covered percentage is only determined by the size of the pore and it is insensitive to the number of the patches. An obvious jump of SCP_A from 25% to 40% occurs at D/L_0=1.8 to 1.9, corresponding to a morphological transition from a virus-like patchy structure to a hybrid structure. This result indicates that the above-mentioned morphological transition could be originated from the large difference between SCP_A and SCP_C. It can be argued that a patchy particle with more than seven patches will have a larger difference between SCP_A and SCP_C, hence that kind of patchy particles are hard to form in such an A- C symmetric system. With a further increase of the pore size, the difference between SCP_A and SCP_C decreases slowly. The average occupied surface-area per patch (S_A) is also plotted in Fig. 3 with a blue line. There are three local minimum values in the S_A curve at D/L_0=0.8, 1.1 and 1.4, which correspond to the changes of the number of the patches from 1 to 2, from 2 to 4 and from 4 to 5, respectively. After each minimum, S_A increases rapidly due to the fact that the pore diameter increases and the number of the patches keeps constant until reaching the next minimum value. With increasing D/L_0 from 1.6 to 1.8, the value of S_A becomes smaller and smaller since that more patches are formed, although the pore diameter is increased.

For triblock copolymers, the chain conformation can be specified with the bridging fraction of the chains (v_B). This fraction should significantly influence the viscoelasticity, mechanical strength, and other physical properties of the triblock copolymers. In our study, the definition of bridging fraction follows that of Wang et al.[64] In brief, the values of bridging fraction corresponding to various morphologies are computed by directly examining each individual chain through calculating the angle (φ) between the vectors from the center of mass of block B to the centers of mass of blocks A and C, as suggested by Huh et al.[65] We consider a chain as a bridge chain if $\cos\varphi \leq 0$ and a loop chain when $\cos\varphi > 0$. The fraction of bridge chain (v_B) is measured by calculating integral of the distribution $cos\varphi$ for $\cos\varphi \leq 0$. We obtained that v_B is about 0.98 for triblock $A_8B_8C_8$ in the bulk phase, which shows the bridge chains are absolutely dominating in the bulk lamellar structure. Under confinement, the variation of v_B as a function of D/L_0 is plotted in Figure 4. As shown in Fig. 4, the bridging fraction for structures under confinement is always

10

smaller than that in the bulk lamellar phase, which indicates that part of the chains tend to curve to form a loop conformation under such confinement. On the other hand, the values of v_B are mostly close to the bulk value at D/L_0=0.7 and 2.5 that correspond to the Janus structure and the partially stacked disks, respectively. This fact indicates that the chain conformation in these two structures is similar to that in the bulk lamellar structure. This observation is not surprising because the Janus structure could be regarded as one-layer stacked disk, and partially stacked disks are partial lamellae, thus they are similar to the bulk lamellar structure. It is also interesting to find that the ratio of bridge chains presents a large decrease when the patch number increases from 1 to 2 and from 2 to 4 at D/L_0=0.8 and 1.1, respectively, and a relatively small decrease at D/L_0=1.4 and 1.7 as the patch number increases from 4 to 5 and from 5 to 6, respectively. For structures with the same number of patches, such as during D/L_0=1.1~1.4 and during D/L_0=1.4~1.6, v_B increases with the increase of D/L_0 due to the fact that polymer chains will more stretch in a larger pore. With a further increase of the pore size, no pronounced decrease of v_B is observed even when a morphological transition occurs. These observations of the variation of v_B provide us two pieces of information. The first one is that polymer chains tend to be in a loop conformation within smaller sized pores because of strongly structural frustration. Conversely, more polymer chains are in a bridging conformation within larger pores due to the release of the frustration. The second one is that more polymer chains tend to be in a loop conformation when the number of patches increases at a given sized pore, such as at D/L_0 = 1.4.

Besides the bridging fraction, we also calculate the mean square end-to-end distance $<d^2_{ee}>$ to gain information of chain conformation in the confined systems. The $<d^2_{ee}>$ as a function of D/L_0 is plotted in Fig. 5. As a comparison, the bulk value is also plotted in the figure. All the $<d^2_{ee}>$ values are measured in unit of the value of the corresponding ideal Gassian chain (with the value of Nb^2, where $b^2 \approx 1.6285$ is the square of the average of all the allowed bond length and N is the corresponding chain length). It is noticed that all the data points in Fig. 5 are much larger than unit, indicating that the chains are much stretched than the corresponding ideal Gaussian chains. This is because the chains are self-avoiding and there are incompatible interactions between different blocks. Secondly, we observe a region of compression of the chains when $D/L_0 \leq 1.6$ and a region of

11

stretching of the chains when $D/L_0 \geq 1.7$. This observation indicates that the confinement effect is stronger in small pores and relatively weaker in large pores, which resembles the conclusion obtained from ν_B curve shown in Fig. 4. In the compression region, we observe three minima in $<d^2_{ee}>$ at D/L_0=0.8, 1.1, and 1.4 which correspond to morphological transitions from Janus structure to P2, from P2 to P4 and from P4 to P5, respectively. From these minima, we can deduce that the patchy structures are frustrated in terms of chain compression. Also, we notice that the minimum values of $<d^2_{ee}>$ curve separate the compression region into three parts. In each part, $<d^2_{ee}>$ increases with D/L_0 almost linearly. In the stretching region, $<d^2_{ee}>$ increases with D/L_0 in the range of D/L_0=1.7~1.8 and $<d^2_{ee}>$ almost keeps constant when D/L_0>1.8, which is similar to the trend of ν_B shown in Fig. 4. Both ν_B and $<d^2_{ee}>$ curves illustrate that the chain conformation is strongly affected in small pores but this effect is weakened with the increase of pore size.

C. *Effects of the wall preference*

In this section, the influences of the interactions between the pore-wall and the terminal A and C blocks on the self-assembled morphologies of linear triblock copolymers $A_8B_8C_8$ confined in spherical pores are systematically investigated. Typical morphologies and a phase diagram as a function of α_A and α_C (where ε_{AW}=-$\alpha_A k_B T_{ref}$ and ε_{CW}=-$\alpha_C k_B T_{ref}$) are plotted in Fig. 6 for the case of a fixed pore diameter of D/L_0=1.3. The pore-wall property is varied from neutral ($\alpha_{A(C)}$=0) to strongly preferential ($\alpha_{A(C)}$= 4.0) to each of the two terminal blocks, where α_A and α_C increase with a small step of 0.1 independently. As shown in Fig 6(a), twelve typical morphologies have been identified and all of them are patchy structures; and for each structure, snapshots of the overall morphology, two individual domain morphologies and a cross-sectional view are given. A phase diagram as a function of α_A and α_C is displayed in Fig. 6(b) for $\alpha_A \leq \alpha_C$ since the phase diagram is symmetric about the axis of $\alpha_A = \alpha_C$. The patches could be formed by either A-blocks or C-blocks when $\alpha_A = \alpha_C$, and as mentioned earlier, we refer the patch-forming block as A block in this case. However, for the other cases with $\alpha_A < \alpha_C$, the patches are always formed by A blocks due to their less wall preference.

As can be seen from Fig 6(b), the number of patches on a particle surface is controlled by the degree of pore-wall preference (α_C), while the internal structure is determined by the wall selectivity to the two terminal blocks (α_C-α_A). For neutral and weakly preferential pore-wall with

α_C =0 ~ 0.4, nanoparticles with two patches (P2) are formed. The structures shown in Fig 6(a) indicate that this P2 structure is slightly different from the P2 structure shown in Fig. 2 at D/L_0=0.8~1.0. In this P2 structure, the A blocks form a dumbbell shaped structure instead of two separated patches and the middle B blocks form a flower-basket shaped structure instead of a flat disk. This P2 structure looks like having two B-rings on the surface, which is due to the weaker wall preference to the terminal blocks. It is interesting to notice that nanoparticles with three patches (P3_a and P3_b) are observed in a small region with α_C≈0.4 ~ 0.6 in Figure 6(b). The difference between P3_b and P3_a is that there are B domains on the surface in P3_b. This difference is originated from the difference of the wall preference. With increasing the strength of the wall preference, four-patch virus-like nanoparticles (P4_a, P4_b and I_P4) are observed in a relatively wider range of α_C (≈ 0.6 ~ 1) region. When the difference between α_A and α_C is less than 0.5, the four-patch virus-like structures, P4_a, have relatively larger patches on the surface. As the difference between α_A and α_C increases, the P4_a structure evolves into the P4_b structure where the size of the patches becomes small due to the less preferential of the wall to the patch-forming A blocks, whereas the centric A-domain core swells and a phase-separated B-C core occurs in the center of the particle. With a further increase of (α_C -α_A) to 0.9, an outermost shell forms with C blocks (shown as transparent in the snapshot), and the patches formed by the A blocks shrink into the inside of the particle, forming an inner four-patch particle and also with a phase-separated B-C core (I_P4). Similarly, for strongly preferential walls with α_C >1.0, five-patch nanoparticles (P5_a) and six–patch (P6_a) virus-like nanoparticles are formed in the ranges of α_A = α_C =1.5 ~ 2.0 and α_A = α_C =2.5 ~ 4.0. When the wall preferential difference to the two terminal blocks increases to 0.5, morphologies P5_a and P6_a are replaced by P5_b and P6_b, respectively, where the P5_b and P6_b are all with a phase-separated B-C core. As the value of α_C - α_A is larger than 1, I_P6 structure consisting of an outermost C-shell (shown as transparent) and inner six patches with a centric phase-separated B-C core spontaneously forms in the nanopore. With a further increase of α_C - α_A to about 2, I_P7 structure with seven inner patches is formed as a degenerated structure with I_P6.

In the limiting case of α_A=α_C, morphological transitions from P2 to P3_a to P4_a to P5_a and finally to P6_a occur with increasing $\alpha_{A(C)}$. We have tested cases with more strongly preferential walls, such as α_A=α_C = 5~10 and the observed structures remain to be P6_a. Therefore, we conclude that the number of the patches on each particle surface is 2 to 6 with an interval of 1. This

result is also verified by performing simulations in smaller and larger nanopores (Fig. S1 in the Supporting Information). For the case with D/L_0=0.9, the number of patches on each particle surface varies from 1 to 2 and to 3 with the increase of α_A. For the case with D/L_0=1.5, this number increases from 2 to 3 to 4 to 5 and finally to 6 with $\alpha_A = \alpha_C = 0 \sim 2.0$.

In order to elucidate the mechanism of the observed morphological transitions, the average contact number between two different components, as well as the surface-covered percentage by the A (SCP_A) and the C (SCP_C) monomers, the bridging fraction, and the mean-square end-to-end distance for the entire chain $<d_{ee}^2>$ and for the three individual chains $<d_{eeA}^2>$, $<d_{eeB}^2>$ and $<d_{eeC}^2>$ are calculated as a function of α_A for the case $\alpha_A=\alpha_C$ for systems with D/L_0=1.3. In Fig 7(a), the average contact numbers for an A- monomer, a B-monomer and a C- monomer with pore-wall sites (n_{AW}, n_{BW} and n_{CW}) are plotted as a function of α_A. It is noticed that n_{BW} decreases from a value of ~1.25 at α_A=0 rapidly to 0 at α_A=0.5 and keeps as zero with a further increase of α_A. It is also noticed that the value of n_{AW} is much smaller than that of n_{CW} due to the difference in structures between the A-domain (patches) and the C-domain (spherically perforated lamella). It is easy to understand that the curve of n_{AW} or n_{CW} has the same tendency as that of the SCP_A or SCP_C curve since that the value of n_{AW} (or n_{CW}) is proportional to the occupied surface-area by the A (or C) monomers. In the range of α_A =0 ~ 0.5, both n_{AW} and n_{CW} increase rapidly, and after that n_{AW} decreases slowly whereas n_{CW} increases slowly. The ultimate value of SCP_A is 25%; and the ultimate value of SCP_C is 75%. Figure 7(b) shows the average contact number between the three kinds of monomers as a function of α_A. As shown in Fig 7(b), the curve of n_{AB} is close to that of n_{BC} and they are much higher than that of n_{AC}. The value of n_{AB} (or n_{BC}) increases in the range of α_A=0 ~ 1.5 and then keeps as a constant with the increase of α_A. However, n_{AC} increases rapidly in the range of α_A =0 ~ 1.0 and then it has two jumps at α_A =1.5 and 2.5 corresponding to the morphological transition from P4_a to P5_a and from P5_a to P6_a, respectively. This is due to the fact that the contact area n_{AC} is proportional to the number of patches on the particle surface.

The variation of bridging fraction (v_B) with α_A is plotted in Fig. 8. As shown in the figure, v_B is always smaller than the bulk value except for the first data point that corresponds to the neutral wall for the three blocks. The overall trend is that, with the increase of α_A, v_B decreases rapidly first, then slowly and finally to a stable value of $v_B = 0.72 \sim 0.73$. On the other hand, we notice that

the whole data points on the ν_B curve can be categorized into five parts (as shown in the dashed circles in Fig. 8) which correspond to structures P2, P3_a, P4_a, P5_a and P6_a, respectively. Different parts are separated by a relatively larger decrease in ν_B value which located at the morphological transition positions at $\alpha_A = 0.4$, 0.7, 1.5 and 2.5, respectively. These observations indicate that the chain conformation is strongly affected by the value of α_A, and the morphological transitions between different patchy structures correlate with the variation of the chain conformation, indicating that the morphological transitions are related to entropy effects. It is also interesting to notice that the effect of α_A is weakened with the further increase of α_A and arrives a threshold at $\alpha_A = 2.5$ where morphology with six patches (P6_a) forms. With a further increase of α_A, the value of ν_B no longer decreases and the number of patches in a self-assembled morphology remains six even at $\alpha_A = 10$.

The mean square end-to-end distance of the entire chain, $<d_{ee}^2>$ as a function of α_A is shown in Fig 9(a). As a comparison, the bulk value is also plotted in the figure. Similar to that in Fig. 5, all the data points in Fig 9(a) are much larger than unit, indicating that the chains are much stretched than the corresponding ideal Gaussian chains. For neutral and weakly preferential walls with $\alpha_A = 0 \sim 0.3$, the values of $<d_{ee}^2>$ for the confined systems are much larger than that in the bulk, indicating that chains are highly stretched in the P2 structure. With increasing α_A, the curve of $<d_{ee}^2>$ drops and the values are close to the bulk value at $\alpha_A = 0.4 \sim 0.6$ within the P3_structure. The reason for the drop of $<d_{ee}^2>$ is that the A and C blocks are attracted to the wall due to the strong wall preference, and the chains close to the wall are compressed since they cannot interpenetrate with other chains from the outward radial direction due to the existence of the wall, which is the same as the cases of diblock copolymers confined in cylindrical and spherical nanopores.[54, 55] When the wall preference is large enough ($\alpha_A \geq 0.7$), the decrease of $<d_{ee}^2>$ becomes slow and the chains are highly compressed (with much smaller $<d_{ee}^2>$) relative to the unconfined chains. Furthermore, the mean square end-to-end distance of the three kinds of individual blocks $<d_{eeA}^2>$, $<d_{eeB}^2>$ and $<d_{eeC}^2>$ as well as their corresponding bulk values are plotted in Fig 9(b). As shown in Fig 9(b), $<d_{eeA}^2>$, $<d_{eeB}^2>$ and $<d_{eeC}^2>$ curves for the confined systems are all larger than their corresponding bulk value in the range of $\alpha_A = 0 \sim 0.3$. While for other α_A values the curves for different blocks are quite different. For the A blocks, $<d_{eeA}^2>$ curve decreases with the increase of α_A; the value of $<d_{eeA}^2>$ is

larger than the corresponding bulk value until α_A =2.0 and smaller than the latter when α_A=2.5 ~ 4.0. For the B blocks, $<d_{eeB}^2>$ increases in the range of α_A=0.1 ~ 0.6 and then decreases slowly with increasing α_A; the value of $<d_{eeB}^2>$ is always larger than its corresponding bulk value. For the C blocks, $<d_{eeC}^2>$ decreases with increasing α_A and the value of $<d_{eeC}^2>$ is always much smaller than the corresponding bulk value when α_A > 0.3. On the other hand, as seen from Fig 9(b), the value of $<d_{eeC}^2>$ is always smaller than that of $<d_{eeA}^2>$ and $<d_{eeB}^2>$, which clearly shows that C-blocks are strongly compressed. This is because that most C-blocks are located in the particle surface.

In summary, it can be concluded that in the range of α_A = 0 ~ 0.3, the P2 structure is energetically favored due to a less contact between incompatible blocks, even though there is an entropic penalty due to chain stretching. On the other hand, the P3_a, P4_a, P5_a and P6_a structures are entropically favored with compressed chains, but they suffer an enthalpy penalty in which there are more A/C contacts. The reason for this is originated from the fact that with increasing the wall preference, more and more terminal blocks are attracted to the particle surface where they are highly compressed. Therefore we conclude that the morphological transitions $P2 \rightarrow P3\_a \rightarrow P4\_a \rightarrow P5\_a \rightarrow P6\_a$ are induced by an entropic effect.

D. *Effects of the copolymer composition*

All the results discussed in the previous sections are obtained for systems with volume fractions of $f_A=f_B=f_C$=1/3. However, the copolymer composition ($f_{A/B/C}$) is another parameter and plays an important role to the outcome of the self-assembly. Typical morphologies and a triangular morphological phase diagram are plotted in Figure 10 for confined systems with a strongly preferential wall ($\alpha_A=\alpha_C$=1), and the pore diameter is fixed at *D*=27 lattice spacing. In Figure 10(a), snapshots of typical morphologies, as well as those for individual domains and a cross-section view, are plotted. In Figure 10(a), only patchy structures with A-patches are plotted for systems with symmetric terminal blocks of f_A= f_C. For systems with asymmetric terminal blocks of f_A< f_C, only patchy structures with A-patches are formed due to an entropy effect.

In Figure 10(b), the value of f_B is varied from 0.25 to 0.75 with a step of 0.0833, f_A is varied from 0.125 to (1− f_B)/2 with a smaller step of 0.0416, and f_C is determined by f_C =1− f_A − f_B. In the top region of the triangular phase diagram, the middle B blocks are the majority, where A- and C-helical stripe structures (H_{AC}) are observed for systems with symmetric terminal blocks (f_A= f_C). The cross-section view of H_{AC} structure reveals that the terminal A and C blocks form a

16

phase-separated centric core and a thin helical striped surface shell, while the middle B blocks form a thick spherical shell located between the core and the surface shell. Furthermore, patchy structures are observed in most region of the phase diagram. As shown in Fig 10(a), comparing to H_{AC} structure, the P6_S structure is composed of a single A-domain centric core, a middle B-shell and a surface shell in which A-patches are distributed in the C-matrix. It is also observed that the number of patches is six and the distribution of the A- patches on the surface shell is highly symmetric. At f_B =0.5, with the decrease of f_A, the equilibrium structure evolves from P6_S to P4_S, which has the same structure but the number of the patches is four in P4_S. In the center region of the triangular diagram with $f_A \approx f_B \approx f_C \approx 1/3$, virus-like patchy structures, P4_a, similar to those observed in Figures 2 and 6, are obtained. On the other hand, a generic morphological transition sequence from P4_a to P4_c to P4_S or to P4_S2 is observed with decreasing f_A. For example, at f_B=0.4165, P4_a is obtained for system with symmetric terminal blocks ($f_A = f_C$); while with the decrease of f_A, the cylindrical tunnels connecting the core and the patches are gradually broken in P4_a, hence P4_c and P4_S form. The P4_S2 structure with a new centric C-domain core is observed with a further decrease of f_A to a rather small value of ~0.125. For systems with f_B=0.083, where the middle B blocks are the minority, the observed morphologies as a function of f_A are relatively complex. At the bottom-left corner of the phase diagram, the terminal C blocks are the majority, where P_AB_9 structure is observed in which the majority C blocks form a matrix while the minority A and B blocks form nine A-B double-layer patches distributed on the surface and a B-A-B triple-layer core located in the center of the pore. As f_A increases to 0.125, P_AB_6 structure is observed in which six uniformly sized A-B double-layer patches are distributed on the surface but without an A/B-domain centric core. With the increase of f_A, the patches become to fuse together and a series of degenerate structures M1, M2 and M3 are obtained. In the range of f_A =0.166 ~ 0.25, two degenerate structures (M1) including striped P3 and stacked ring structures are observed. In the range of f_A=0.292 ~ 0.333, two degenerate structures (M2) including P3 and striped P2 structures are observed. When the terminal bocks are nearly symmetric (f_A =0.375~0.458), four degenerate structures (M3) including P2, P3_a, lamellae perpendicular to one of the axis pore and shake-hand structures are spontaneously formed. It is interesting to notice that the case with $f_A \approx f_C$, $f_B \to 0$ corresponds to the system where symmetric diblock copolymers confined in the non-selective nanopores. In our previous studies[55], the structures of P2, P3_a, lamellae perpendicular to one of the

axis pore structures are observed when symmetric diblock copolymers confined into neutral or weakly preferential nanopores. However, the shake-hand structure is never found in our previous studies. The formation of the shake-hand structure may be due to the existence of the middle B-blocks and/or the strongly preferential wall to both of the terminal blocks.

Despite the complexity of the morphologies and the morphological transition sequence, some generic features of the phase behavior can be extracted from the phase diagram shown in Figure 10(b). The first generic feature is that the self-assembled morphology is mainly governed by the volume fraction of the middle B blocks (f_B). Regular patchy nanoparticles with six patches and/or four patches spontaneously form when f_B is moderate. When f_B is much larger than f_A and f_C, the patchy structures degenerate into helical stripe structures H_{AC}. On the contrary, as f_B is much smaller than f_A and f_C, a series of degenerated structures are observed and the patch shapes on the surface including circles, ring and strips which is analogous to the case of diblock copolymers confined in spherical nanopores. The second generic feature of the phase behavior is that the internal morphology is largely controlled by the volume fraction ratio of two terminal blocks (f_A/f_C). A general morphological transition sequence $P4\_a \rightarrow P4\_c \rightarrow P4\_S \rightarrow P4\_S2$ is observed with the decrease of the ratio f_A/f_C where the cylindrical tunnels connecting the patches and the centric core are broken gradually in P4_a, hence P4_c and P4_S form, and finally a new C-domain core occurs in the center of P4_S2. Moreover, when f_B approaches to 0, a set of degenerate structures are obtained in the region of $f_A \approx f_C$. This is consistent with the case when symmetric diblock copolymers are confined in spherical nanopores with neutral or weakly preferential walls.[55]

E. *Comparison with related experimental results*

Our simulation results can be compared with some related experiments. However, to the best of our knowledge, there has been no report on experimental studies of the self-assembly of linear triblock copolymers confined in spherical nanopores. One related system is micelles self-assembled from linear triblock copolymers dissolved in a selective solvent.[25-30] Multiple multicompartment micelles are observed in experiments from the micro-phase separation between the two hydrophobic blocks[25] or hydrophilic blocks[29]. However, a selective solvent was often used in these experiments so that the polymer-solvent interactions are different from the polymer-wall interactions used in our simulations. Another related system is polymer nanoparticles, formed by block copolymers

18

confined in droplets. Recently, Higuchi and co-workers exhibited a series of results about the micro-phase separated nanoparticles formed by bulk lamella-forming diblock copolymers confined in droplets.[66, 67] It was found that Janus nanoparticles are observed when D/L_0 is smaller than 1.0, and nonlamellar micro-structures such as screw-like, mushroom, wheel-like and tennis ball structures are formed when $1.0 < D/L_0 < 2.0$. Especially, lamellar structure similar to the bulk phase becomes the observed structure when $D/L_0 > 2.1$.[66] Comparing their experimental results with those obtained from our simulations, a distinct feature can be clearly seen. As shown in Fig. 2, Janus structures and a series of nonlamellar (patchy) structures are predicted when $D/L_0 \leq 2.0$. When the pore size increases to D/L_0=2.5, roughly lamellar structures are formed. This common structural feature indicates that the confinement effect is strong for small pores and weakened for large pores. Due to the consistency between experiment and simulation, we can conclude that a critical pore size for the forming of patchy particles is $D/L_0 \approx 2.0$ for bulk lamellae-forming block copolymers in a 3D confinement and the nonlamellar micro-structures are caused by the small size effect.[68] The differences between the nonlamellar structures obtained from our simulation and from their experiment can be obviously attributed to the different block copolymers used in the studies.

On the other hand, it is noticed that the phase behavior should be similar to diblock copolymer when the component of B- blocks closes to zero. As shown in Fig. 10, a series of degenerated structures such as shake-hand, P2 and P3_a structures are predicted when B- component is much smaller than that of A and/or C. These predicted structures are similar to the tennis-ball, mushroom and screw structures observed in experiment of Higuchi and co-workers.[66] In contrast, when B component is much larger than that of A and C blocks, a new core-shell structure with an outermost helical shell and Janus-type domain in the center region predicted in our simulation has never been reported before. Another class of novel confinement-induced structures predicted in our simulations is the Janus-type patchy structures, such as P_AB_6 and P_AB_9 shown in Fig. 10(a) in which the component of C block is much larger than that of A and B blocks. These Janus type patchy structures may be exclusively confinement-induced structures of triblock copolymers, which could not be observed for diblock copolymers in the 2D- or 3D-confinement.

Conclusion

We have systematically investigated the self-assembly of linear ABC triblock copolymers

19

confined in spherical nanopores when the pore-wall prefers to the terminal A and C blocks using a simulated annealing method. Multiple types of patchy nanoparticles with switchable surfaces are observed. The distribution of the patches on the surface of a given particle is highly symmetric. The number of patches on a nanoparticle surface increases with increasing the pore diameter as well as with increasing the wall selectivity. The shape of each patch depends on the pore-wall preferences to the blocks and the composition of the copolymer. Multiple morphological transitions are predicted.

For the bulk lamella-forming triblock copolymers $A_8B_8C_8$ confined in pores with strongly preferential walls, a series of virus-like patchy nanoparticles with 1, 2, 4, 5, 6 and 7 patches on the surface are predicted with increasing the pore size to $D/L_0 =1.8$, whereas when $D/L_0 \geq 1.9$, patchy structures no longer occur. Therefore, the patchy structures obtained at $D/L_0 \leq 1.8$ are regarded as frustrated structures. This phenomenon is consistent with that observed experimentally in diblock copolymer nanoparticles. It is found that the difference in surface-covered percentages of A and C monomers increases with the increase of D/L_0 for the patchy particles, indicating that A- and C-domain shapes are quite different although A- and C- blocks are symmetric both in composition and in interactions in these systems. It is deduced that a patchy particle with more than seven patches is hard to form in an A- C symmetric system. The phase diagram with typical patchy nanoparticles has been constructed through systematically varying the wall preferences to the two terminal blocks. In the limiting case of $\alpha_A = \alpha_C$, a morphological transition sequence of $P2 \rightarrow P3\_a \rightarrow P4\_a \rightarrow P5\_a \rightarrow P6\_a$ is predicted. These morphological transitions are attributed to the entropic effect through analyzing the average contact number between different components, and chain conformation from calculating the bridging fraction and the mean square end-to-end distance of the chain. As the difference between the wall preferences to the two terminal blocks increases, the morphological transition sequences of the P*3*_a to the P2 or the P*4*_a and to the P3_b usually occur when the wall preferences are relatively weak, and the morphological transition sequences of the P*n*_a to the P*n*_b and to the I_P*n* usually occur when the wall preferences are relatively strong.

The effects of the copolymer composition to the self-assembled morphologies are investigated and a phase diagram is constructed for confined systems with a strongly preferential wall. Two generic features of the phase behavior are obtained. Firstly, the overall self-assembled morphology

is governed by the volume fraction of the middle B blocks. With the decrease of f_B, the pattern on the particle surface transforms from helices to patches and to degenerated structures including circular, ring-like and striped patches. Secondly, the internal morphology is largely controlled by the volume fraction ratio of the two terminal blocks, f_A/f_C. With the decrease of f_A/f_C, a morphological transition sequence $P4\_a \rightarrow P4\_c \rightarrow P4\_S \rightarrow P4\_S2$ is predicted.

Our investigation suggests a simple routine for fabricating "smart nanoparticles" with unique patchy structures. The patchy structures can be controlled by tuning parameters such as the size of nanopore, the pore-wall preference and the copolymer composition. Our study illuminates that the number of patches on a particle can be precisely tuned by the pore size and the strength of pore-wall preference. Moreover, a number of new morphologies such as H_{AC} with a helical shell and Janus-like shell have also been predicted. Novel patchy nanoparticles with complex geometries are supposed to be potentially useful in subsequent hierarchical self-assembly, preparing of bio-mimetic material, biological drug delivery and other particle-base technologies.

Supporting Information Available: In the limiting case of $\alpha_A=\alpha_C$, self-assembled morphologies as a function of α_A for triblock copolymers $A_8B_8C_8$ confined in nanopores with $D/L_0=0.9$ (Figure S1(a)) and $D/L_0=1.5$ (Figure S1(b)), respectively.

Figure caption

Figure 1. Snapshot of alternative lamellae formed from linear triblock copolymers $A_8B_8C_8$ in bulk simulation with a box of $38\times40\times42$. Color scheme in this and the following Figures: A blocks (red), the middle B blocks (green) and C blocks (blue).

Figure 2. Self-assembled morphologies as a function of D/L_0 for triblock copolymers $A_8B_8C_8$ confined in pores with $\varepsilon_{AW}=\varepsilon_{CW}=-1.0k_BT_{ref}$. From the bottom to the top, the overall view, and the structures of A-domain viewed from two different directions ($D/L_0=1.1\sim1.8$), B-domain and C-domain are shown. For the Janus nanoparticle at $D/L_0=0.7$, a cross-section view is also given for clarity.

Figure 3. The surface-covered percentage of the terminal (A and C) blocks and the average patch area as a function of D/L_0 for triblock copolymers $A_8B_8C_8$ confined in pores with $\varepsilon_{AW}=\varepsilon_{CW}=-1.0k_BT_{ref}$. The lines with circular symbols represent the surface-covered percentage of the A (black line) and C (red line) monomers, they correspond to the left Y-axis in the unit of percentage. The line with triangular symbols represents the average patch area, it corresponds to the right Y-axis in the unit of square of lattice spacing.

Figure 4. The bridging fraction as a function of D/L_0 for triblock copolymers $A_8B_8C_8$ confined in pores with $\varepsilon_{AW}=\varepsilon_{CW}=-1.0k_BT_{ref}$. The corresponding typical morphologies are also shown.

Figure 5. The mean square end-to-end distance $<d^2_{ee}>$ as a function of D/L_0 for triblock copolymers $A_8B_8C_8$ confined in pores with $\varepsilon_{AW}=\varepsilon_{CW}=-1.0k_BT_{ref}$. The corresponding bulk value is plotted as a line.

Figure 6. Self-assembled morphologies as functions of α_{AW} and α_{CW} for triblock copolymers $A_8B_8C_8$

confined in pores with D/L_0=1.3. (a) Twelve typical morphologies are clearly demonstrated through displaying the overall, the individual (A, B, and C) domain and a cross-section views. In order to illustrate the internal structures, the surface shell formed by the C blocks is shown as transparent for I_P4, I_P6 and I_P7 structures. (b) The phase diagram as functions of α_A and α_C. The same symbols represent similar morphologies.
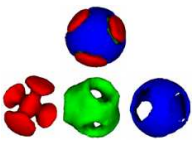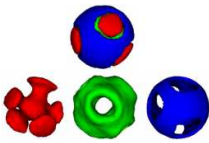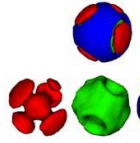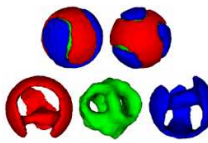
Figure 7. For the case of α_A=α_C, (a) the average contact number (left Y-axis) between the pore-wall and the individual (A, B and C) blocks and the surface-covered percentage (right Y-axis) as a function of α_A; (b) the average contact numbers between the individual (A, B and C) blocks as a function of α_A.

Figure 8. The bridging fraction as a function of α_A when α_A=α_C. The corresponding typical morphologies are also shown.

Figure 9. The mean-square end-to-end distances as a function of α_A for the case of α_A=α_C, and the corresponding bulk values are plotted as lines. (a) $<d_{ee}^2>$, (b) $<d_{eeA}^2>$,$<d_{eeB}^2>$ and $<d_{eeC}^2>$.

Figure 10. For systems with α_A=α_C=1 and pore diameter D=27 lattice spacing. (a) Typical self-assembled morphologies. H_{AC}: helical striped structure; P6_S: six separated patches on the surface + one centric core; P4_a: four patches on the surface +one centric core +four cylindrical tunnels; P4_c: some of the cylindrical tunnels are broken in comparison with P4_a; P4_S: four patches on the surface + one centric core; P4_S2: a new centric C-domain core occurs in comparing with P4_S; P_AB_9: nine A-B double-layer patches on the surface + a B-A-B triple-layer centric core; P_AB_6: six A-B double-layer patches on the surface; M1: degenerate structures: two polar patches and an equatorial circle + three uniform lengthened patches; M2: degenerate structures: two polar patches + P3_a; M3: degenerate structures: P2 + P3_a + lamellae perpendicular to one of the axis pore + shake-hand. (b) The composition triangular phase diagram. The same symbols represent similar morphologies, and the typical morphologies with overall and A-domain views are shown.

Table 1 The possible morphologies and the corresponding occurring probability at D/L_0=1.4.

Name	**P4**	**P5**	**H1**	**H2**
Overall and A-, B- and C-domain snapshots				
Occurring probability	59%	41%		

Figure 1

24
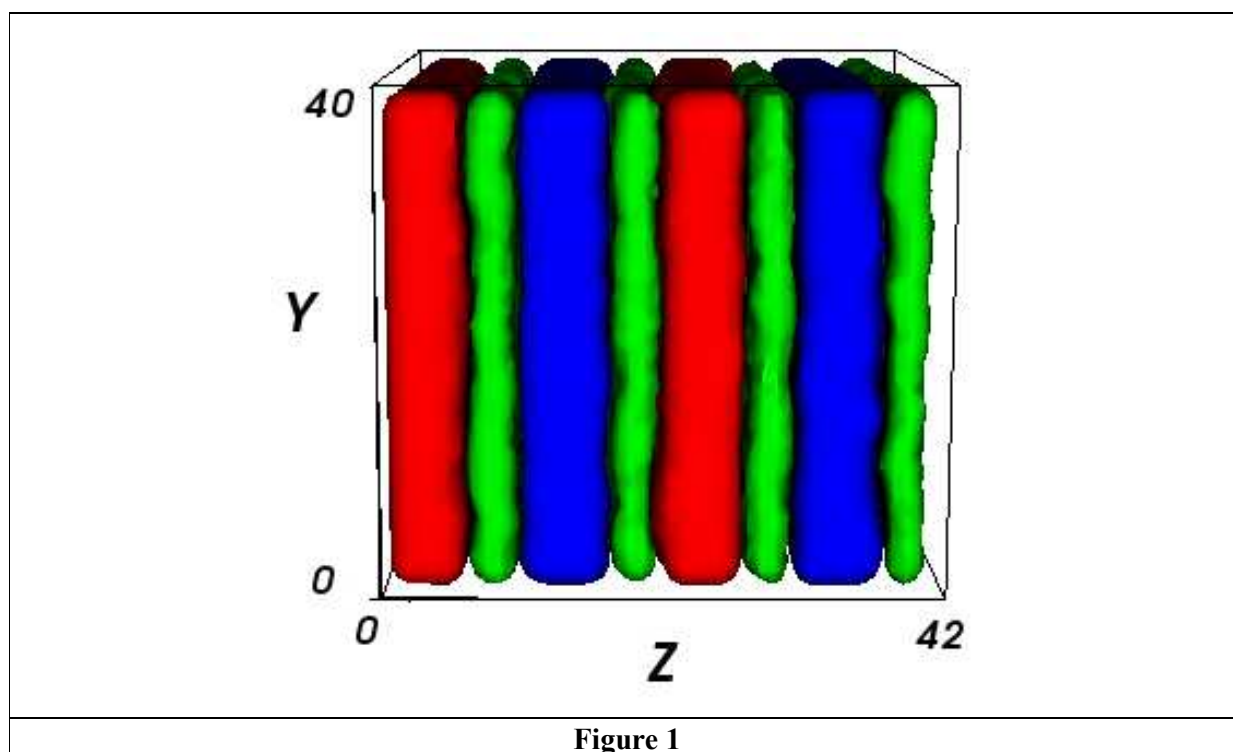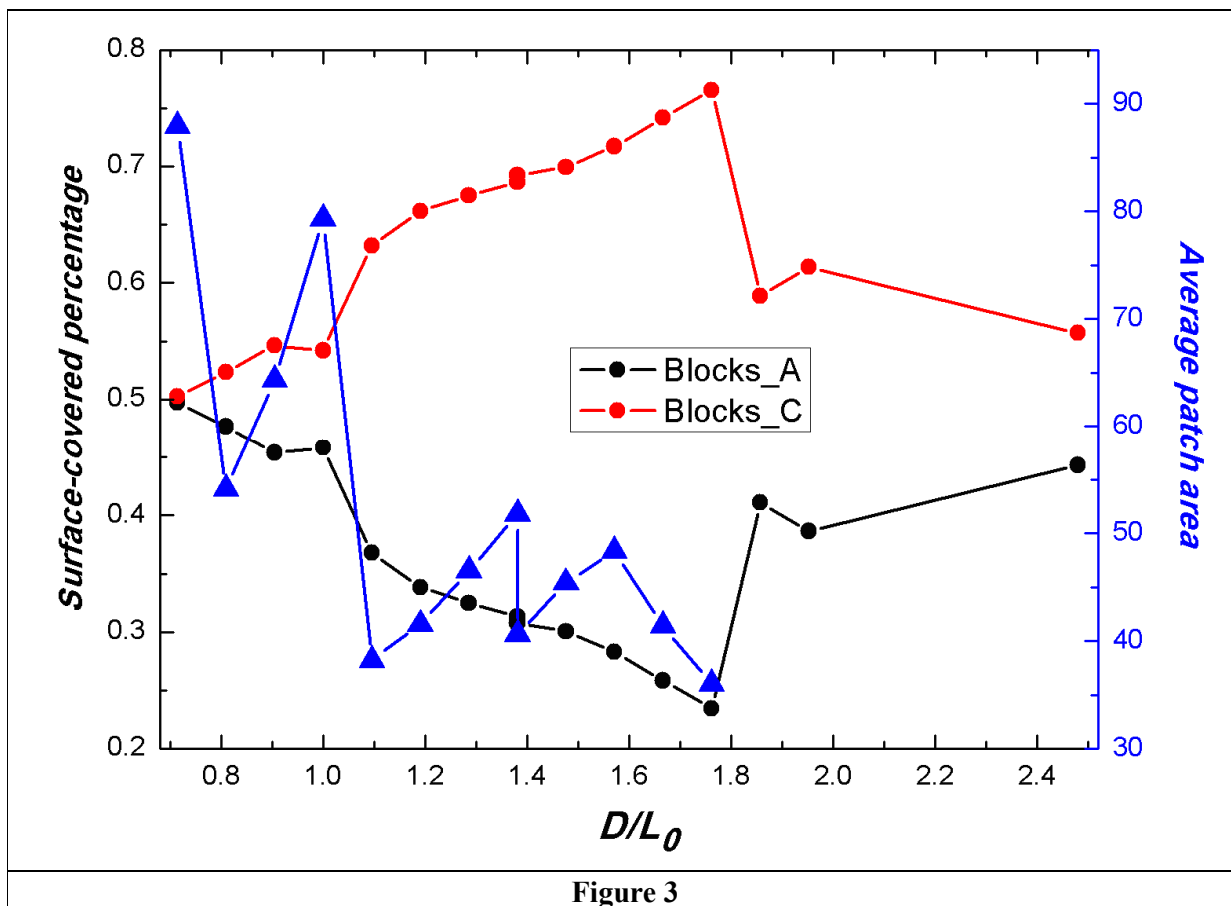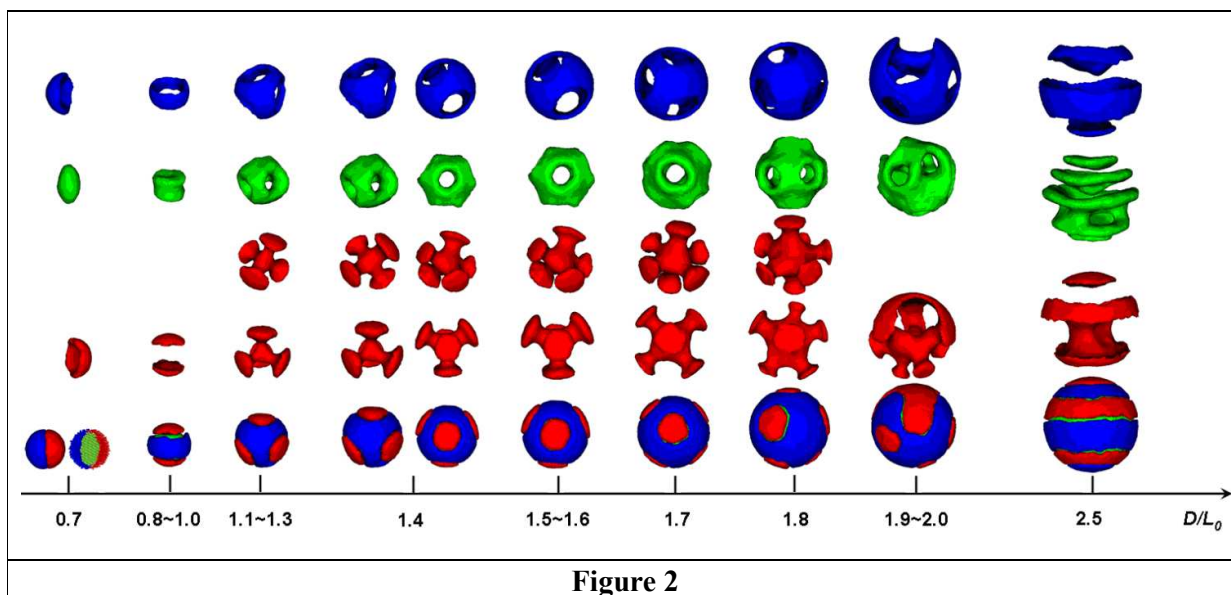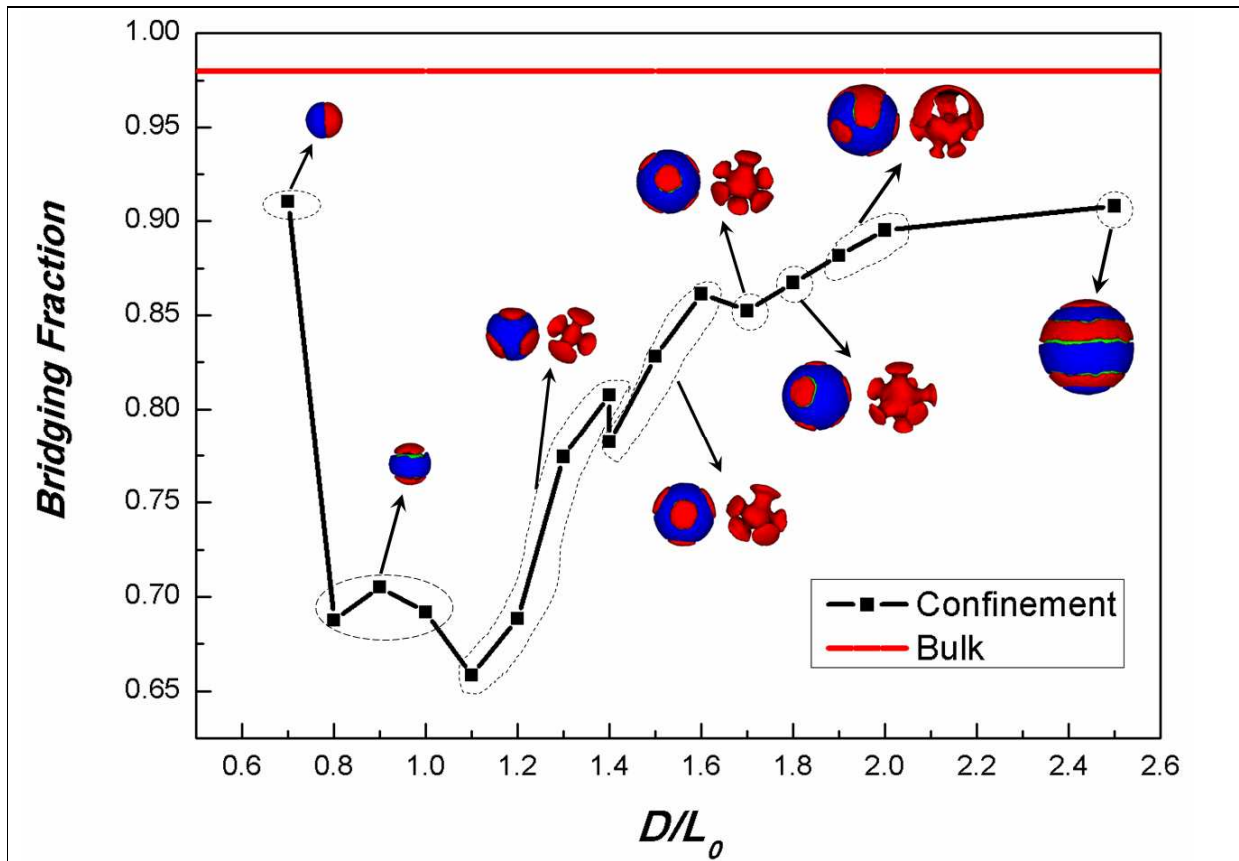
Figure 2

Figure 3

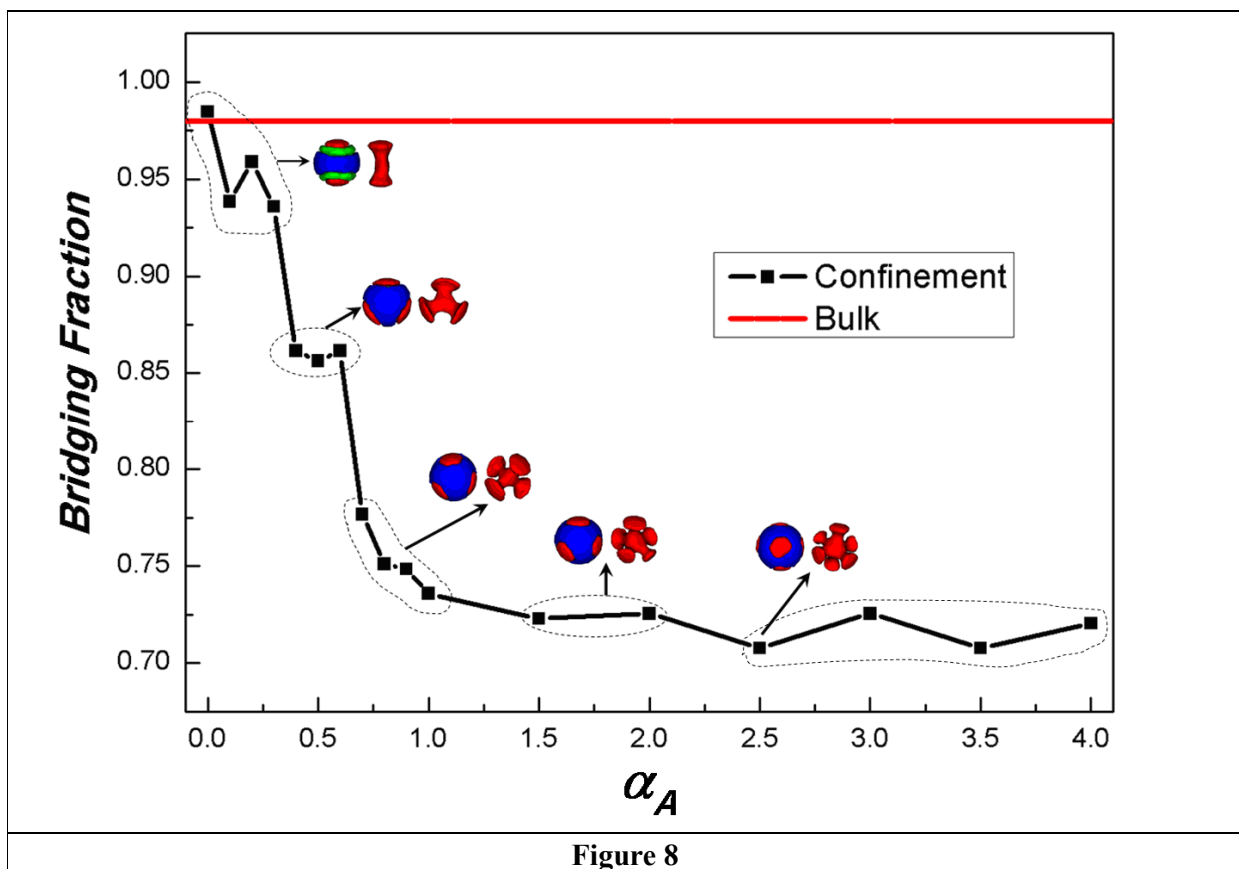**Figure 4**

Figure 5

Figure 6
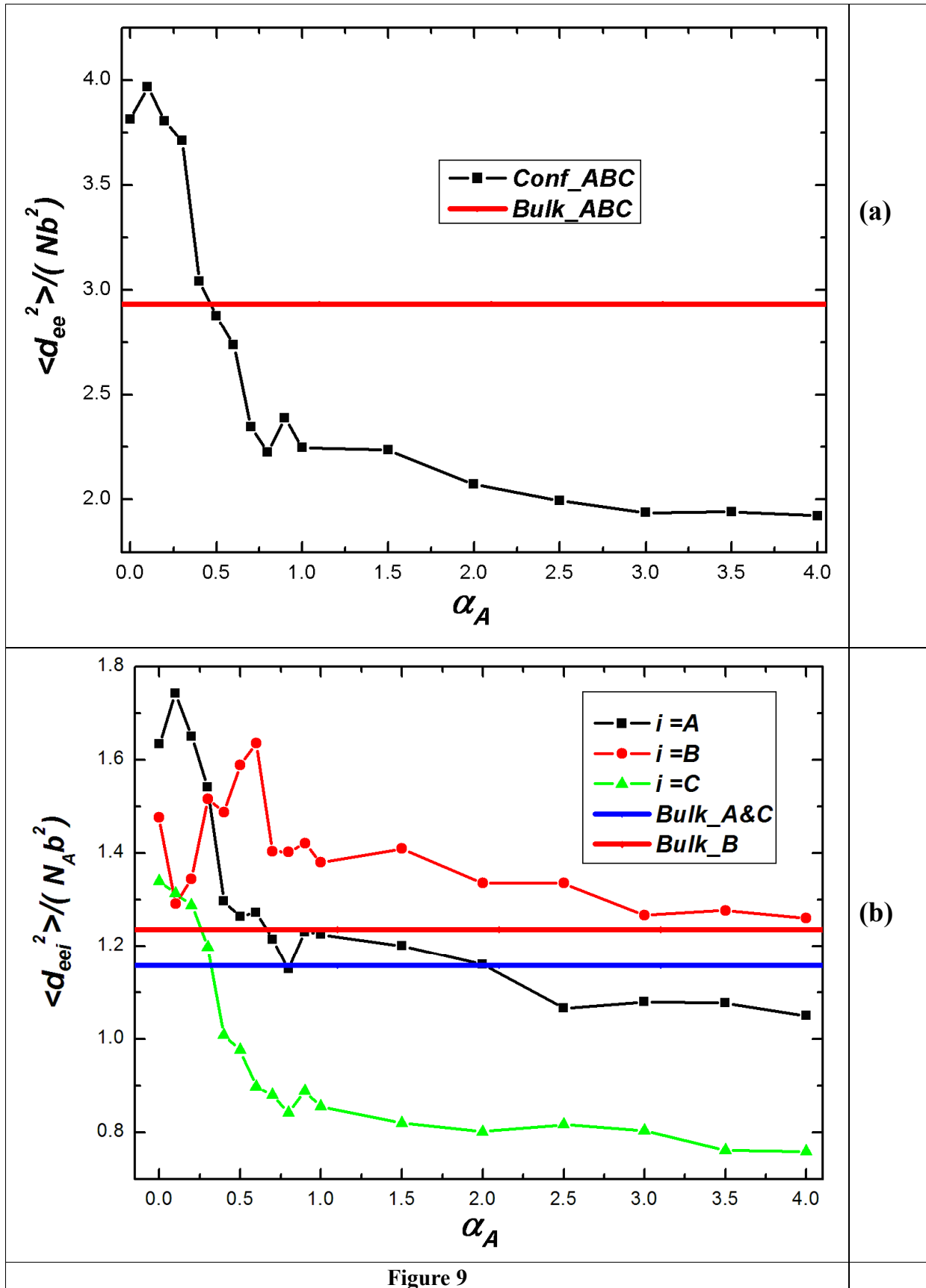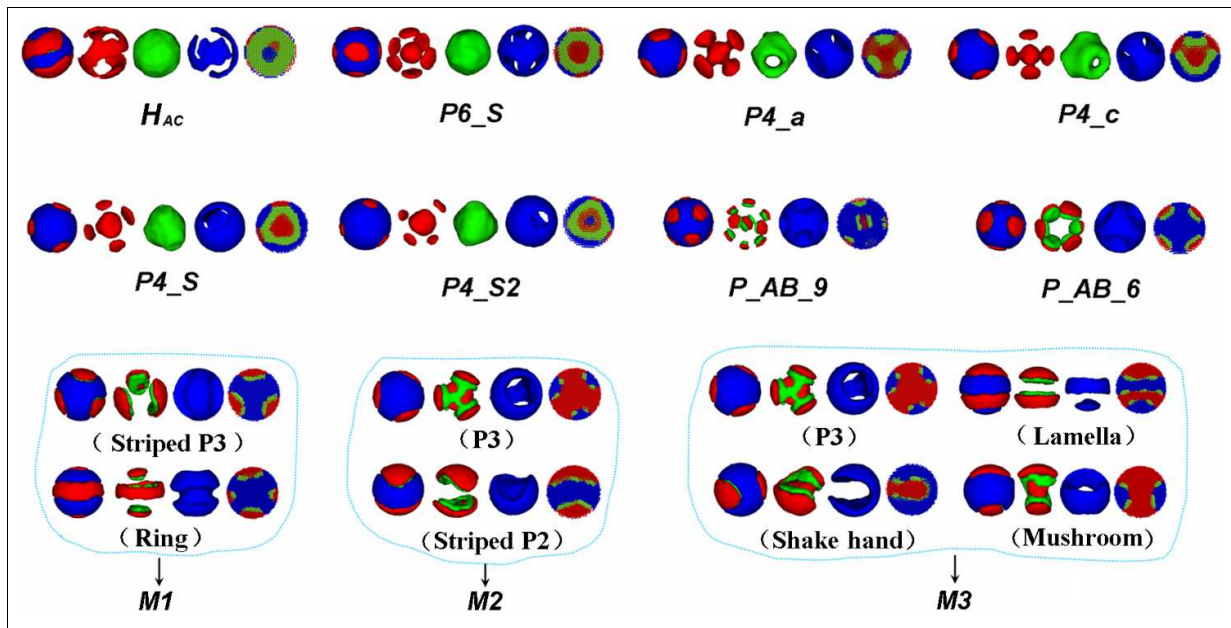
27
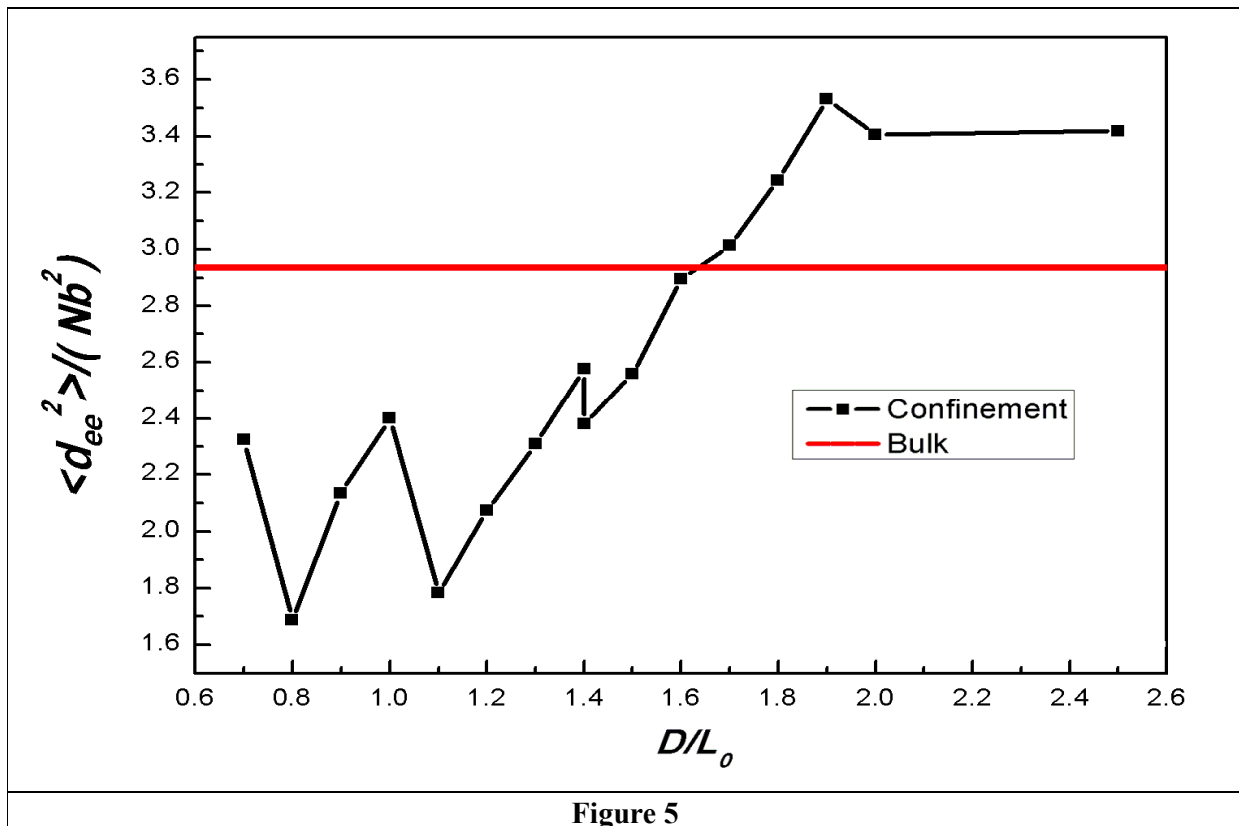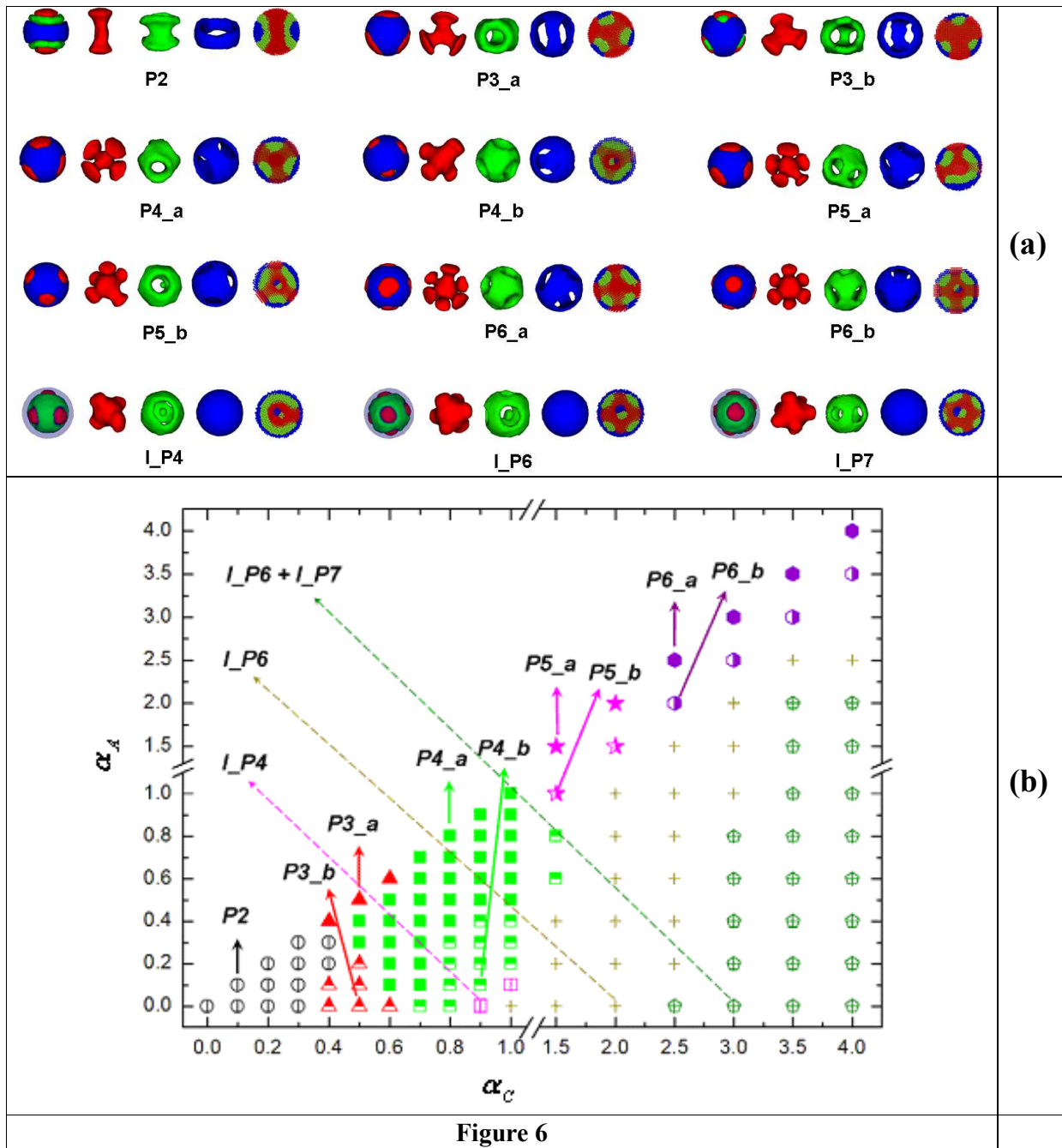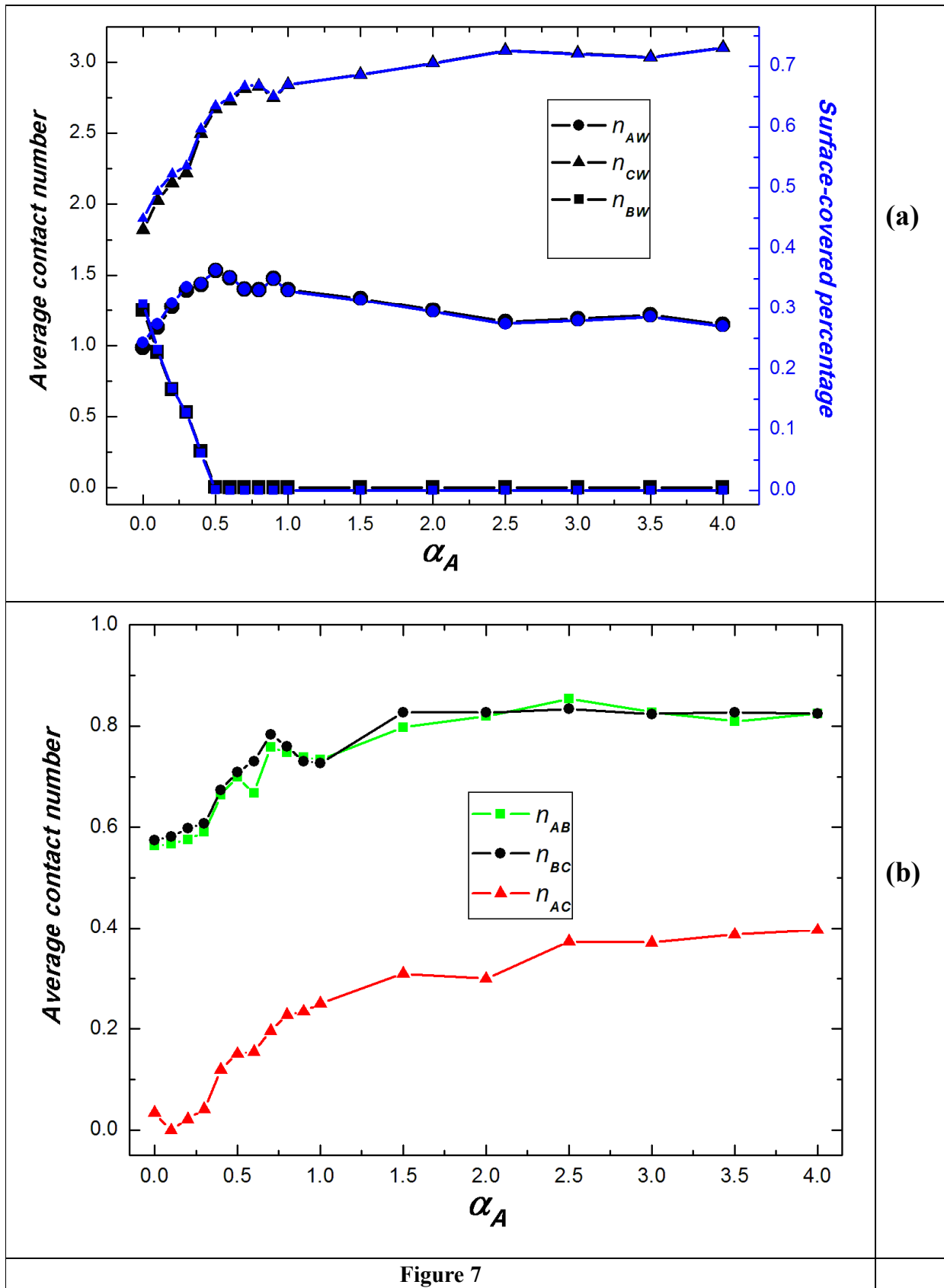
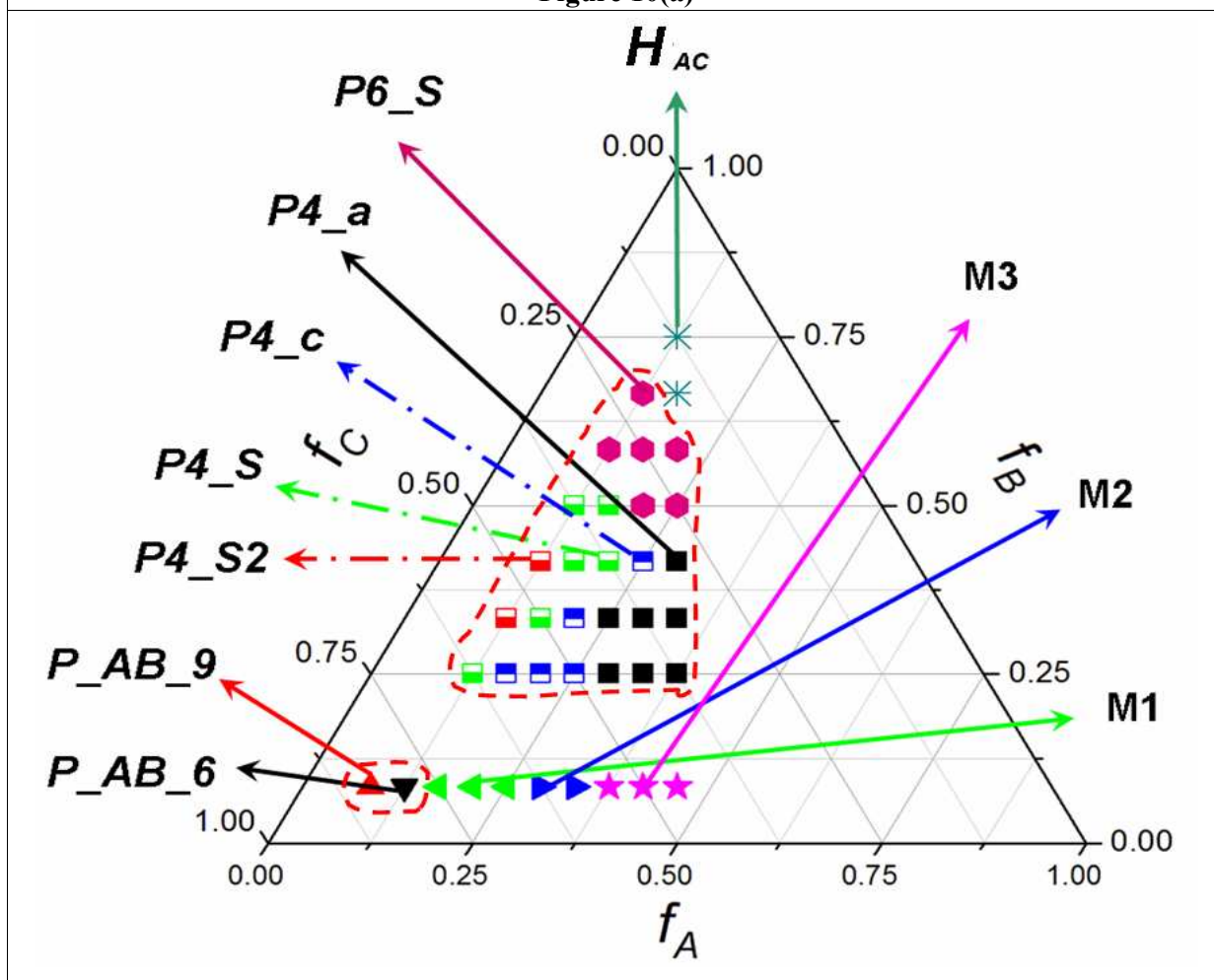Figure 7

Figure 8

Figure 9

Figure 10(a)

Figure 10(b)

31

References

1. P. S. Weiss, *Acs Nano*, 2008, **2**, 1085-1087.
2. S. C. Glotzer, *Science*, 2004, **306**, 419-420.
3. S. C. Glotzer and M. J. Solomon, *Nat. Mater.*, 2007, **6**, 557-562.
4. E. Duguet, A. Desert, A. Perro and S. Ravaine, *Chem. Soc. Rev.*, 2011, **40**, 941-960.
5. J. Z. Du and R. K. O'Reilly, *Chem. Soc. Rev.*, 2011, **40**, 2402-2416.
6. A. Walther and A. H. E. Muller, *Soft Matter*, 2008, **4**, 663-668.
7. F. Wurm and A. F. M. Kilbinger, *Angew. Chem.-Int. Edit.*, 2009, **48**, 8412-8421.
8. S. Jiang, Q. Chen, M. Tripathy, E. Luijten, K. S. Schweizer and S. Granick, *Adv. Mater.*, 2010, **22**, 1060-1071.
9. M. Zhengwei, X. Haolan and W. Dayang, *Adv. Funct. Mater.*, 2010, **20,** 1053-1074.
10. A. B. Pawar and I. Kretzschmar, *Macromol. Rapid Commun.*, 2010, **31**, 150-168.
11. Z. L. Zhang and S. C. Glotzer, *Nano Lett.*, 2004, **4**, 1407-1413.
12. J. F. Lutz and A. Laschewsky, *Macromol. Chem. Phys.*, 2005, **206**, 813-817.
13. T. Nisisako, T. Torii, T. Takahashi and Y. Takizawa, *Adv. Mater.*, 2006, **18**, 1152-1156.
14. R. Langer and D. A. Tirrell, *Nature*, 2004, **428**, 487-492.
15. M. Yoshida and J. Lahann, *Acs Nano*, 2008, **2**, 1101-1107.
16. A. Alexeev, W. E. Uspal and A. C. Balazs, *Acs Nano*, 2008, **2**, 1117-1122.
17. Z. L. Zhang, A. S. Keys, T. Chen and S. C. Glotzer, *Langmuir*, 2005, **21**, 11547-11551.
18. R. Erhardt, A. Boker, H. Zettl, H. Kaya, W. Pyckhout-Hintzen, G. Krausch, V. Abetz and A. H. E. Mueller, *Macromolecules*, 2001, **34**, 1069-1075.
19. R. Erhardt, M. F. Zhang, A. Boker, H. Zettl, C. Abetz, P. Frederik, G. Krausch, V. Abetz and A. H. E. Muller, *J. Am. Chem. Soc.*, 2003, **125**, 3260-3267.
20. L. Hong, A. Cacciuto, E. Luijten and S. Granick, *Nano Lett.*, 2006, **6**, 2510-2514.
21. L. Hong, A. Cacciuto, E. Luijten and S. Granick, *Langmuir*, 2008, **24**, 621-625.
22. L. Nie, S. Y. Liu, W. M. Shen, D. Y. Chen and M. Jiang, *Angew. Chem.-Int. Edit.*, 2007, **46**, 6321-6324.
23. L. Cheng, G. Z. Zhang, L. Zhu, D. Y. Chen and M. Jiang, *Angew. Chem.-Int. Edit.*, 2008, **47**, 10171-10174.
24. F. S. Bates and G. H. Fredrickson, *Phys. Today*, 1999, **52**, 32-38.
25. S. Kubowicz, J. F. Baussard, J. F. Lutz, A. F. Thunemann, H. von Berlepsch and A. Laschewsky, *Angew. Chem.-Int. Edit.*, 2005, **44**, 5262-5265.
26. G. Y. Li, L. Q. Shi, R. J. Ma, Y. L. An and N. Huang, *Angew. Chem.-Int. Edit.*, 2006, **45**, 4959-4962.
27. G. Njikang, D. H. Han, J. Wang and G. J. Liu, *Macromolecules*, 2008, **41**, 9727-9735.
28. M. Uchman, M. Stepanek, K. Prochazka, G. Mountrichas, S. Pispas, I. K. Voets and A. Walther, *Macromolecules*, 2009, **42**, 5605-5613.
29. J. Z. Du and S. P. Armes, *Soft Matter*, 2010, **6**, 4851-4857.
30. E. Betthausen, M. Drechsler, M. Fortsch, F. H. Schacher and A. H. E. Muller, *Soft Matter*, 2011, **7**, 8880-8891.
31. G. Srinivas and J. W. Pitera, *Nano Lett.*, 2008, **8**, 611-618.
32. W. Kong, W. Jiang, Y. Zhu and B. Li, *Langmuir*, 2012, **28**, 11714-U11713.
33. G. J. A. Sevink, A. V. Zvelindovsky, J. Fraaije and H. P. Huinink, *J. Chem. Phys.*, 2001, **115**, 8226-8230.

34. X. H. He, M. Song, H. J. Liang and C. Y. Pan, *J. Chem. Phys.*, 2001, **114**, 10510-10513.

35. K. Shin, H. Q. Xiang, S. I. Moon, T. Kim, T. J. McCarthy and T. P. Russell, *Science*, 2004, **306**, 76-76.

36. H. Q. Xiang, K. Shin, T. Kim, S. I. Moon, T. J. McCarthy and T. P. Russell, *Macromolecules*, 2004, **37**, 5660-5664.

37. Y. M. Sun, M. Steinhart, D. Zschech, R. Adhikari, G. H. Michler and U. Gosele, *Macromol. Rapid Commun.*, 2005, **26**, 369-375.

38. J. Feng and E. Ruckenstein, *Macromolecules*, 2006, 39, 4899-4906.

39. B. Yu, P. Sun, T. Chen, Q. Jin, D. Ding, B. Li and A. C. Shi, *Phys. Rev. Lett.*, 2006, **96**, 138306.

40. W. H. Li and R. A. Wickham, *Macromolecules*, 2006, 39, 8492-8498.

41. M. Ma, V. Krikorian, J. H. Yu, E. L. Thomas and G. C. Rutledge, *Nano Lett.*, 2006, **6**, 2969-2972.

42. P. Chen, H. Liang and A.-C. Shi, *Macromolecules*, 2007, **40**, 7329-7335.

43. Q. Wang, *J. Chem. Phys.*, 2007, **126**, 024903.

44. P. Dobriyal, H. Q. Xiang, M. Kazuyuki, J. T. Chen, H. Jinnai and T. P. Russell, *Macromolecules*, 2009, **42**, 9082-9088.

45. Y. Wang, Y. Qin, A. Berger, E. Yau, C. He, L. Zhang, U. Goesele, M. Knez and M. Steinhart, *Adv. Mater.*, 2009, **21**, 2763-2766.

46. C. R. Stewart-Sloan and E. L. Thomas, *European Polymer Journal*, 2011, **47**, 630-646.

47. I. Carmesin and K. Kremer, *Macromolecules*, 1988, **21**, 2819-2823.

48. R. G. Larson, *J. Chem. Phys*, 1989, **91**, 2479-2488.

49. R. G. Larson, *J. Chem. Phys*, 1992, **96**, 7904-7918.

50. S. Kirkpatrick, C. D. Gelatt and M. P. Vecchi, Jr, *Science*, 1983, **220**, 671-680.

51. S. Kirkpatrick, *J. Stat. Phys.*, 1984, **34**, 975-986.

52. G. S. Grest, C. M. Soukoulis and K. Levin, *Phys. Rev. Lett.*, 1986, **56**, 1148-1151.

53. A. Chakrabarti and R. Toral, *Phys. Rev. B.*, 1989, **39**, 542-545.

54. B. Yu, P. Sun, T. Chen, Q. Jin, D. Ding, B. Li and A. C. Shi, *J. Chem. Phys.*, 2007, **127**, 114906.

55. B. Yu, B. Li, Q. Jin, D. Ding and A. C. Shi, *Macromolecules*, 2007, **40**, 9133-9142.

56. B. Yu, B. Li, Q. Jin, D. Ding and A. C. Shi, *Soft Matter*, 2011, **7**, 10227-10240.

57. T. S. Bailey, *Thesis, University of Minnesota*, 2001.

58. C. A. Tyler, J. Qin, F. S. Bates and D. C. Morse, *Macromolecules*, 2007, **40**, 4654-4668.

59. Z. J. Guo, G. J. Zhang, F. Qiu, H. D. Zhang, Y. L. Yang and A. C. Shi, *Phys. Rev. Lett.*, 2008, **101**, 028301.

60. Y. Matsushita, M. Tamura and I. Noda, *Macromolecules*, 1994, **27**, 3680-3682.

61. T. A. Shefelbine, M. E. Vigild, M. W. Matsen, D. A. Hajduk, M. A. Hillmyer, E. L. Cussler and F. S. Bates, *J. Am. Chem. Soc.*, 1999, **121**, 8457-8465.

62. H. Huckstadt, T. Goldacker, A. Gopfert and V. Abetz, *Macromolecules*, 2000, **33**, 3757-3761.

63. M. Sun, P. Wang, F. Qiu, P. Tang, H. Zhang and Y. Yang *Phys. Rev. E.*, 2008, **77**, 016701.

64. Z. Wang, B. Li, Q. Jin, D. Ding and A. C. Shi, *Macromol. Theory Simul.*, 2008, **17**, 301-312.

65. J. Huh, W. H. Jo and G. ten Brinke, *Macromolecules*, 2002, **35**, 2413-2416.

66. T. Higuchi, A. Tajima, K. Motoyoshi, H. Yabu and M. Shimomura, *Angew. Chem.-Int. Edit.*, 2008, **47**, 8044-8046.

67. T. Higuchi, K. Motoyoshi, H. Sugimori, H. Jinnai, H. Yabu and M. Shimomura, *Soft Matter*, 2012, **8**, 3791-3797.

68. A. C. Shi and B. Li, *Soft Matter*, 2013, **9**, 1398-1413.

For Table of Contents Use Only

Patchy nanoparticles self-assembled from linear triblock copolymers under spherical confinement: A simulated annealing study

Bin Yu, Jianhua Deng, Baohui Li, An-Chang Shi
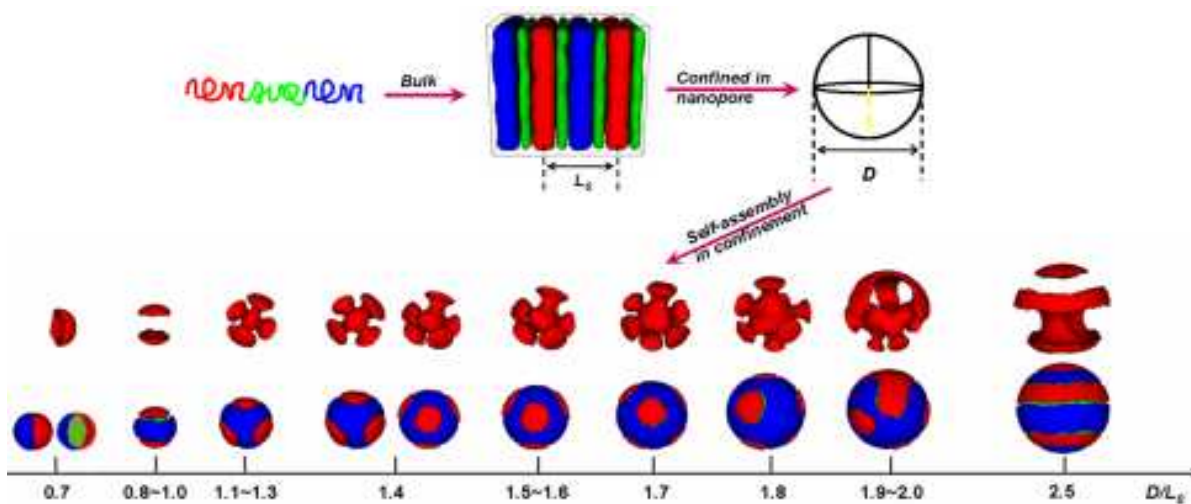
Multiple patchy nanoparticles spontaneously form from self-assembly of triblock copolymers inside spherical nanopores of different sizes or different pore-wall selectivity.

1   Supporting Information for

2   # Patchy nanoparticles self-assembled from linear triblock

3   # copolymers under spherical confinement: A simulated

4   # annealing study

5   Bin Yu, Jianhua Deng, Baohui Li, An-Chang Shi

6

Fig S1
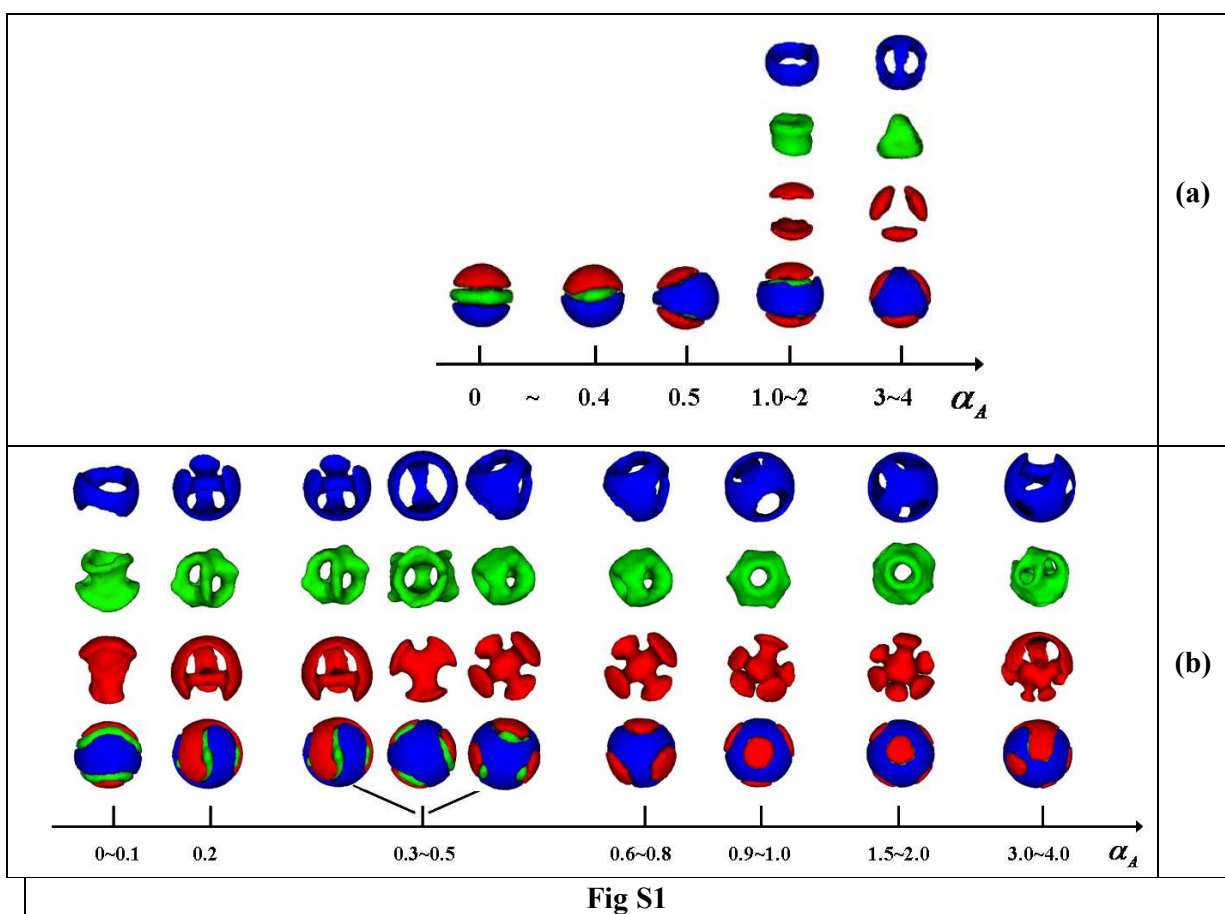
7

8   Figure S1. Self-assembled morphologies as a function of α_A for triblock copolymers $A_8B_8C_8$

9   confined in nanopores with $\alpha_A=\alpha_C$. (a) D/L_0=0.9; (b) D/L_0=1.5.

10